AIR FORCE INSTITUTE OF TECHNOLOGY

AIR UNIVERSITY
UNITED STATES AIR FORCE

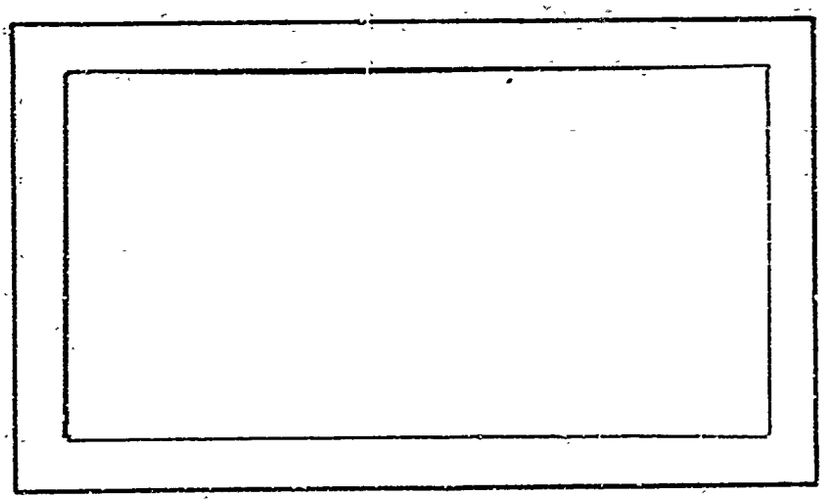

SCHOOL OF ENGINEERING

WRIGHT-PATTERSON AIR FORCE BASE, OHIO

AFLC-WPAFB-AUG 68 6M

DETERMINATION

OF SPALLATION THRESHOLDS

BY EXPLODING FOIL TECHNIQUES

THESIS

GNE/PH/68-2 José R. Baca
Captain USAF

AFLC-WPAFB-AUG 68 35

DETERMINATION OF SPALLATION THRESHOLDS BY EXPLODING FOIL TECHNIQUES

THESIS

Presented to the Faculty of the School of Engineering of
the Air Force Institute of Technology

Air University

in Partial Fulfillment of the
Requirements for the Degree of

Master of Science

by

José R. Baca, B.S.Ch.E.
Captain USAF

Graduate Nuclear Engineering

June 1968

Preface

The thesis research was performed under the direction of the Physics Group at the Air Force Weapons Laboratory at Kirtland AFB, New Mexico. Every single member of the group provided assistance that led to the completion of this project, but there are certain individuals that must particularly be mentioned. The contributions by the personnel at the Pulse Power Facility were profitable, and the data could not have been obtained without the aid of TSgt Bobby D. Wade. Captain John T. Viola, thesis advisor at Kirtland, and Captain Joseph B. Webster provided initial guidance of the research and preliminary critique of the thesis report. The metallurgical results could not have been achieved without the analyses of Mr. John E. Cooney. I must also mention the support and encourgement supplied by my thesis advisor from the Air Force Institute of Technology, Prof. J. A. Wilson.

Captain José R. Baca

Contents

Contents

List of Figures

List of Figures

List of Tables

Abstract

Exploding foil techniques were used to accelerate a Mylar flyer at a controlled velocity to produce a plane, longitudinal shock wave in 6061-T6 aluminum, and the interaction of the wave with the target free surface was studied.

Flyer velocity and planarity were determined by high-speed, photographic techniques. The spall threshold was determined as a function of flyer velocity and thickness. A criterion was formulated to predict the spall threshold.

Microscopic analyses revealed the mechanism of incipient spall in 6061-T6 aluminum to be cracks which propagated from inclusions in the matrix material.

DETERMINATION OF SPALLATION THRESHOLDS BY EXPLODING FOIL TECHNIQUES

I. Introduction

Problem Statement

Requirements exist to formulate fracture criteria for shock wave interactions at free surfaces for different materials. Fracture caused by the reflection of a shock wave from a free surface is defined as spalling or scabbing (Ref 23:315). This study produced a criterion that allowed spall predictions for a structural alloy, 6061-T6 aluminum. Specifically, this research involved material spallation induced by a high-pressure, short duration pulse in a specimen.

This problem was significant since it was directly applicable to the determination of the vulnerability of a re-entry vehicle to a high-pressure, compressive pulse with a short duration. Pulse simulation was obtainable experimentally by impacting a flat flyer plate on a flat parallel target. A capacitor storage system was used to accelerate a Mylar flyer, enclosed in an exploding foil assembly, at a controlled velocity to impact a 6061-T6 aluminum target. The shock waves produced were propagated through the target with the possibility of causing spall.

The impact of two plates, finite in thickness creates a condition of one-dimensional strain. The compression waves generated in both the flyer and target propagate through the material until they reach a free surface and are reflected. When a wave is incident on a free surface, the reflected wave changes its nature. In the case of the target material, a reflected tension wave propagates until it interacts with the compression wave reflected from the flyer-target interface. If the net result of these two stress waves was a tension, it was then possible for a spall surface to form at this point of interaction. Spallation occurred if the resulting tension was greater than the dynamic tensile strength. In general, a time delay for spalling occurs in ductile materials which should not exist for brittle materials.

The evaluation of material damage resulting from the interaction of shock waves at free surfaces and material boundaries has been explored by many investigators. When making scientific investigations on the effects of explosives, Hopkinson, in 1914, observed an interesting phenomenon which has since been termed a Hopkinson Fracture, spalling, or scabbing (Ref 23:315). Serious study of spalling was not started until the 1950's, and no validated damage criterion has been formulated which is amenable to inclusion in material response computations pertinent to

re-entry vehicles. Such a criterion is vitally needed in light of present problems to allow for reliable predictions of material damage.

Problem Analysis

A thorough review and evaluation of the literature was essential to determine what previous efforts had been made. Several surveys were available, and the Engineering Index was researched. The literature search is summarized in Appendix A.

In order to simplify the problem it was necessary to assume that a square shock wave was produced when the flyer impacted the target. By choosing the proper plate dimensions, one-dimensional strain was introduced in which the edge effects were minimal. The target material was a metal for which the assumptions of homogeneity and isotropicity were valid.

The flyer velocity and the flyer impact planarity were determined by photographic techniques. Thus, data reduction depended heavily on the interpretation of film data. Macroscopic and microscopic analyses were necessary to determine the degree of spall damage in the recovered targets. A criterion for spall was formulated by considering the damage threshold of the material with flyer velocity as a function of flyer thickness. The flyer velocity and thickness can be converted to peak pressure and pulse duration, respectively.

II. Theory

Introduction

The production of shock waves by dynamic impact by the exploding foil method leads to plane wave interactions that differ from the static loading efforts. One-dimensional flow and one-dimensional strain may be produced, and the initial and shocked states of a material may be related by a set of jump conditions. Graphical methods have been developed that are essential for the solution of shock wave problems. The assumptions and boundary conditions required for a spallation study must be accurate and complete.

Waves

Planar impacts upon plates of infinite extent produce plane, longitudinal waves which subject the material to uniaxial strain. In general, there are two types of stress pulses generated by an impulsive load (Ref 24:5): a longitudinal pulse in which the particle motion is parallel to the direction of propagation of the pulse and the strain is a pure dilatational disturbance and a transverse pulse in which the strain is in the nature of shear. In a transverse pulse, the particle motion is normal to the direction of propagation of the pulse. In practically all situations, it is sufficient to consider only longitudinal disturbances in which particle motion is in the same direction as progress of the wave front (Ref 23:317). When

considering longitudinal disturbances, two velocities are important, the propagation velocity of the disturbance and the particle velocity. The particle velocity is that velocity with which a point in the material moves as the disturbance moves across it (Ref 24:7).

Plate impact causes waves and wave interactions in the target material. When two waves traveling in opposite directions come together, the resulting stress is obtained by the principle of superposition (Ref 26:2).

One-Dimensional Flow

The propagation of plane, longitudinal waves results from the planar collision of two flat, parallel plates of infinite extent (Ref 6:979). Under these conditions, net strains are confined to the finite or x dimension and wave interactions do not involve partition of the stress waves into longitudinal and shear wave components. The infinite medium in the y and z direction will assure that the net strain in these directions is zero, even though the lateral stresses are non-zero. As long as the measurements or effects are recorded prior to the arrival of release waves (edge effects) from the y and z boundaries, the one-dimensional criterion is satisfied (Ref 6:979).

Ideally, the pressure pulses produced by the impact of a flyer plate against a stationary, parallel target plate are one-dimensional, plane, souare waves. A square wave has a plateau of constant pressure. In front of this

plateau is the vertical shock front and behind the plateau is a vertical rarefaction that falls off to zero pressure.

Jump Conditions

Spalling processes occur according to the dictates of the three fundamental conservation laws of physics, namely, those of mass, momentum, and energy. Consider a plane shock front traveling at constant velocity, C, into stationary material at pressure or stress Po, density ρ_o, and specific internal energy Eo, Fig. 1 (Ref 7:8). The frame of reference for the shock wave is the material or Lagrangian Coordinates where the frame moves with the wave, The material is accelerated to a particle velocity, u_p, by passage of the shock front and compressed to a density $\rho > \rho_o$. The state of the shocked material is related to the initial state by a set of jump conditions that represent the conservation of mass, momentum, and energy in the shock transition:

$$\rho_o C = \rho(C - u_p) \qquad \text{conservation of mass} \qquad (1)$$

$$P - P_o = \rho_o C u_p \qquad \text{conservation of momentum} \qquad (2)$$

$$P u_p = \rho_o C(E - E_o + \frac{u_p^2}{2}) \qquad \text{conservation of energy} \qquad (3)$$

The term $\rho_o C$ is termed the impedance and is symbolized as Z. Eqs (1) and (2) are used to eliminate u_p and C from Eq (3), and the result is called the Rankine-Hugonoit relation:

$$E - E_o = \frac{1}{2}(V_o - V)(P + P_o) \qquad (4)$$

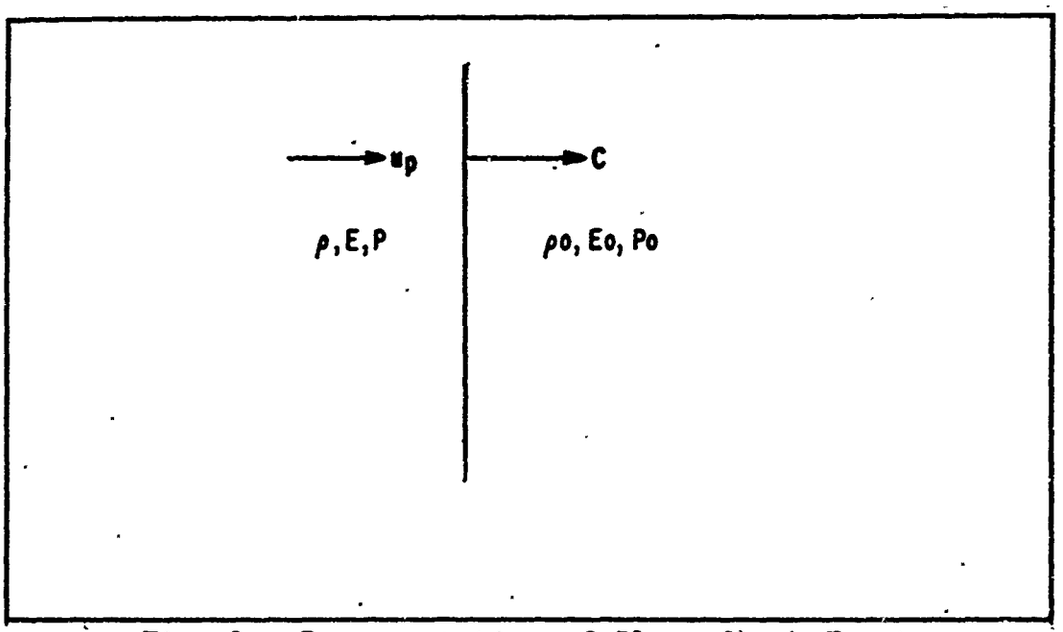

Fig. 1. Representation of Plane Shock Front

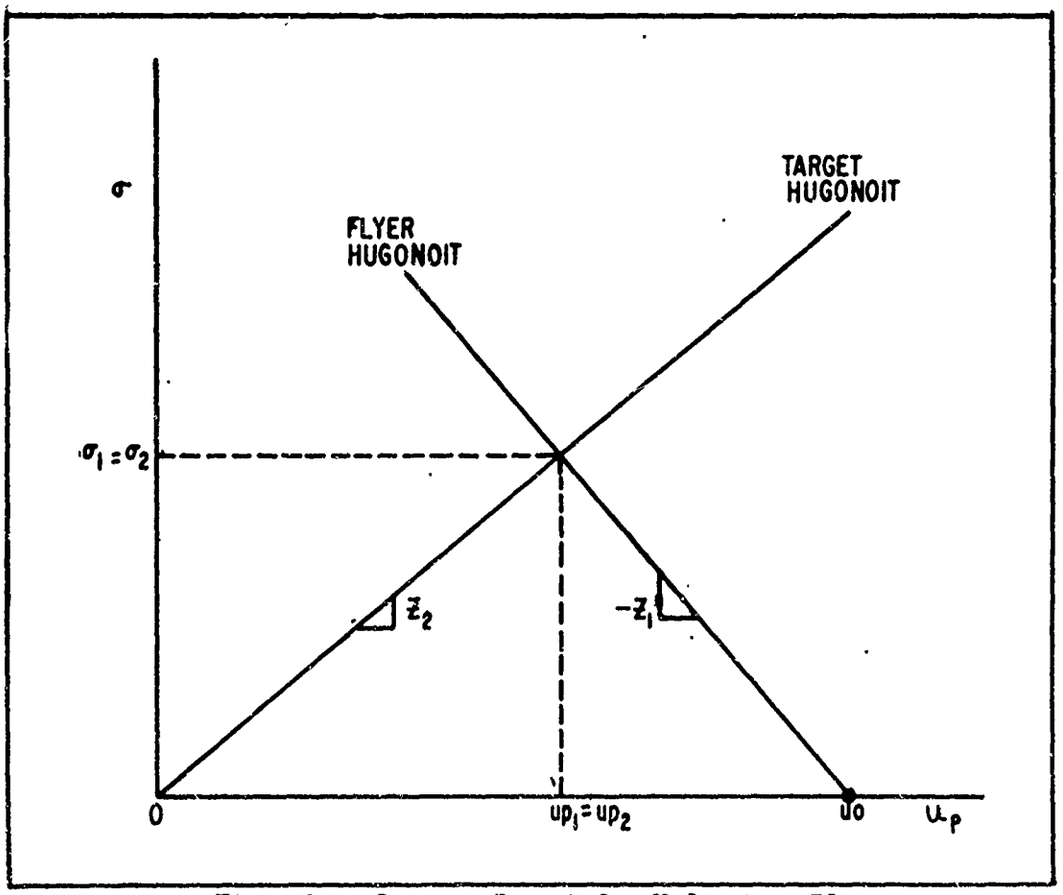

Fig. 2. Stress-Particle Velocity Plot

where V is the specific volume. These equations include five parameters of the shocked state which are C, u_p, ρ, P, and E; one more relation, an equation-of-state, is required before specification of one parameter enables calculation of the other four (Ref 7:9).

If the equation-of-state is given in the form $E = f(P,V)$, it is combined with Eq (4) to yield a relation between P and V known as the Hugonoit. This Hugonoit relation is precise and unique, and it represents the locus of all points which may be reached by a shock transition from the initial state. It is important to understand the distinction between the Hugonoit and other P-V relations because of its importance in determining equations-of-state at very high pressures by means of shock wave techniques (Ref 7:9).

Graphical Representations

Representation of a pulse is accomplished in several different ways. There are two vertical and two horizontal axes for representation of a shock wave (Ref 24:88). Either stress or time is plotted as the ordinate, and either particle velocity or distance is plotted as the abscissa. Flyer velocity plotted against flyer thickness was used. When the appropriate equation-of-state data become available, the initial flyer velocity can be converted to stress and the flyer thickness to time. For these data conversions, it is essential to have an

understanding of time versus distance diagrams and stress versus particle velocity diagrams.

Fig. 2 shows a stress versus particle velocity diagram. The point zero on this diagram represents the stationary target (stress and initial velocity are zero) which has an impedance of Z_2. When the flyer plate impacts the target plate, the conservation of momentum, Eq (2), illustrates the fact that the greater the resulting particle velocity, the greater the resulting stress. As the particle velocity increases, the corresponding stress must follow along the line whose slope is Z_2 beginning at the origin. The final stress and particle velocity are somewhere on this line. The initial particle velocity of the projectile is U_o and the corresponding stress is zero. When the projectile impacts the target, the particle velocity of the projectile decreases and the stress increases. The stress and particle velocity relationship is determined by the line whose slope is $-Z_1$, and the final stress and final particle velocity are somewhere on that line. Since the final stress and the final particle velocity of the two materials are equal, the point where the two impedance lines intersect defines the only conditions that can exist after impact (Ref 13).

The top portion of Fig. 3 shows an interface after impact with the shock waves emerging from the interface at various times. The shock waves propagate at their dilatational velocities. Below this impact configuration, a time versus distance diagram is shown. This diagram

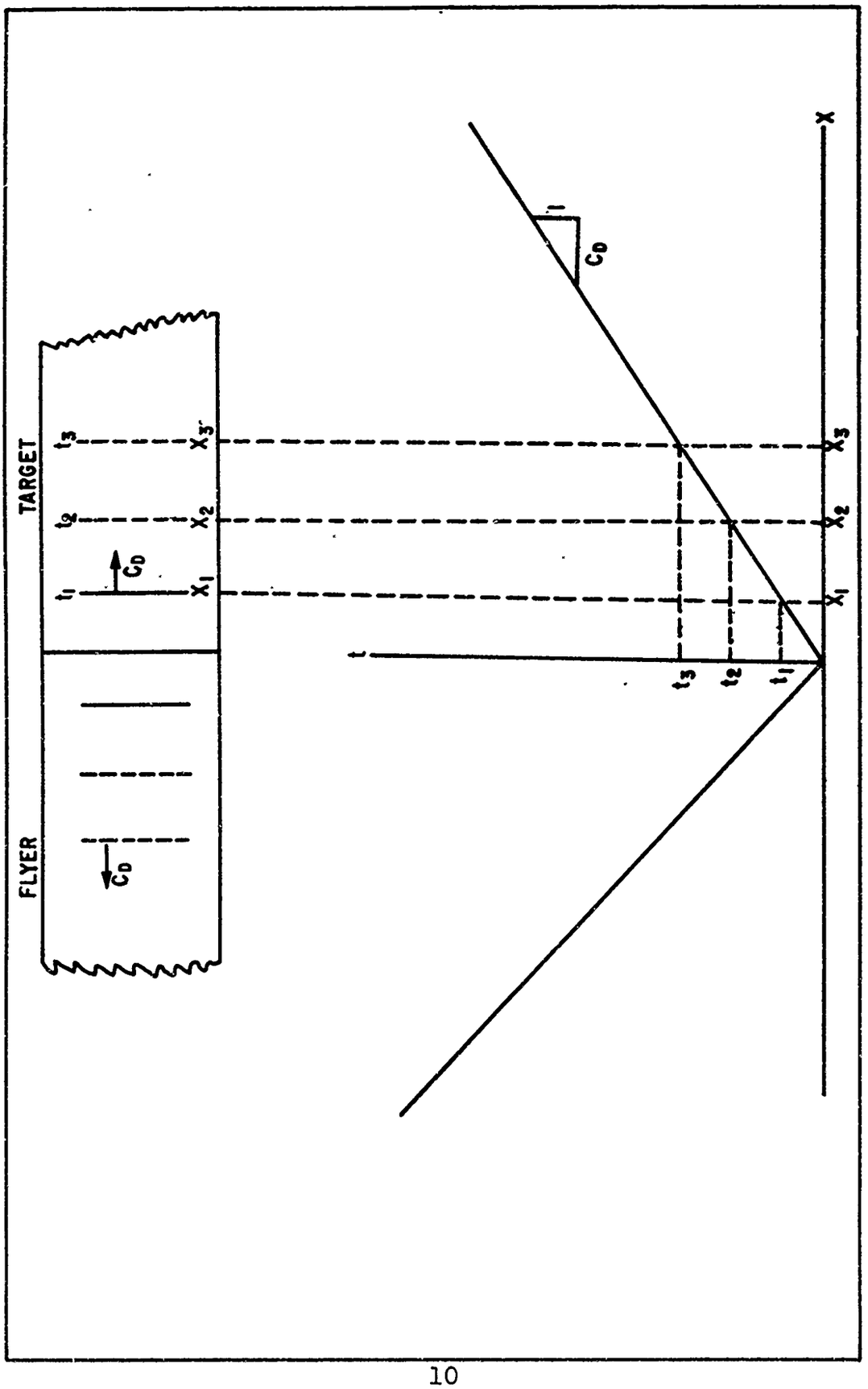

Fig. 3. Propagation of Shock Wave Represented by Time-Distance Plot

shows the two different waves emerging from the interface and shows the progress of the wave through the material. It can easily be deduced that the slope of the line representing the propagation of the wave through a material is equal to the reciprocal of the dilational wave velocity (Ref 13).

A knowledge of the relationships between time versus distance and stress versus particle velocity diagrams can be useful in dynamic, impact problems. Fig. 4 has both types of diagrams, and the following narrative will discuss the relations between both diagrams. The time versus distance diagram is discussed first. At time t_1, the projectile, Z_1, has not impacted the target, and the two are still separated. The lines 1, 2, 3, and 4 are characteristic lines. A characteristic line is a line that defines a discontinuity in pressure, particle velocity, or internal energy. Regions a, b, and c are regions in which no discontinuities can exist because no characteristic lines cross the regions. In region a, the pressure and particle velocity are zero and u_0, respectively, corresponding to the point a on the stress versus particle velocity diagram. In region b, the pressure and particle velocity are both zero corresponding to point b on the stress versus particle velocity diagram. Point 6 is a point in material Z_2 at t_1. As time increases, the first characteristic that crosses position 6 is line 3 taking the material Z_2 from region b to region c.

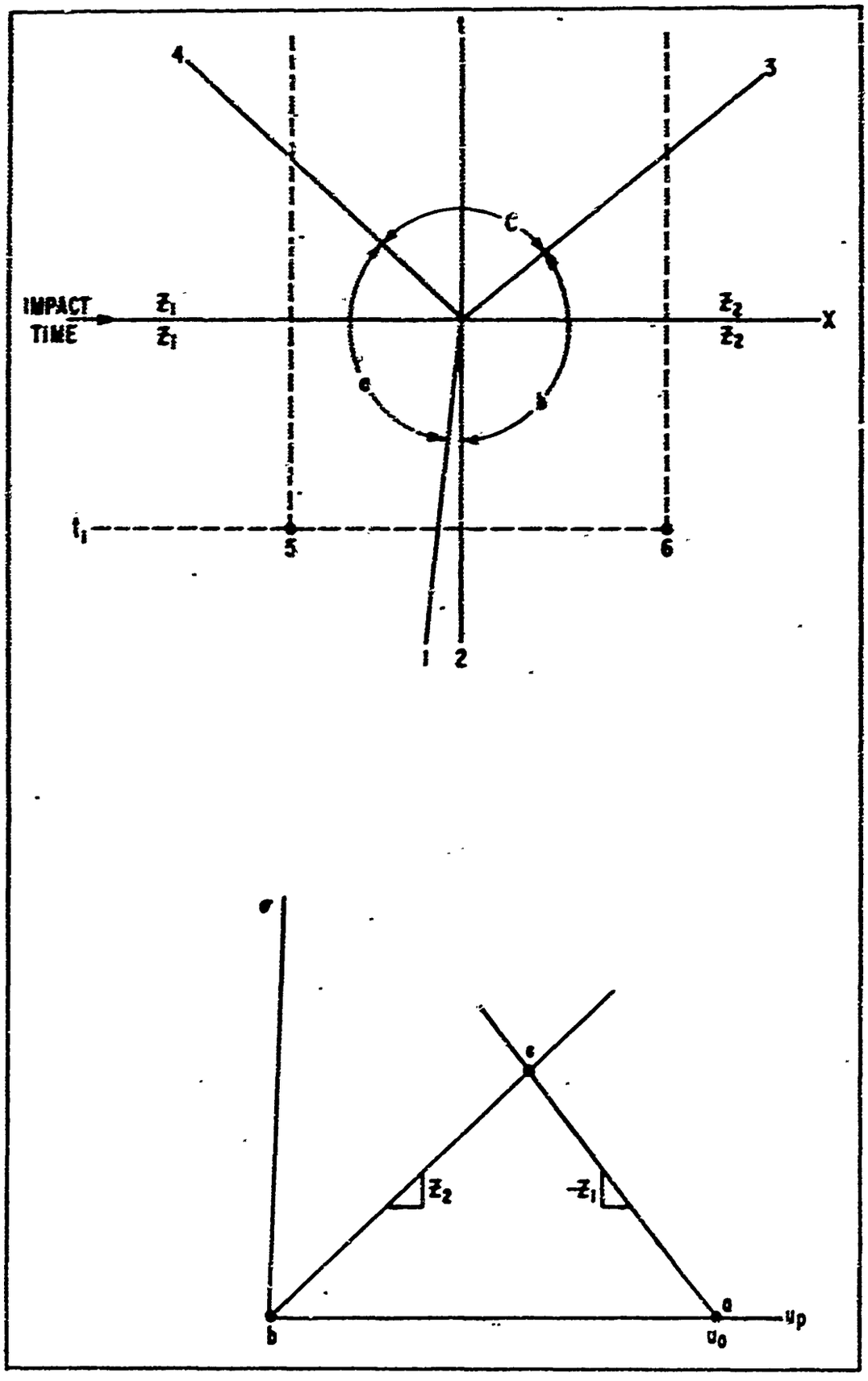

Fig. 4. Relationships Between Time-Distance and Stress-Particle Velocity Plots

Characteristic 3 has a positive slope; therefore, the path on the stress versus particle velocity plot from point b to point c must also have a positive slope, Z_2. Starting at t_1 from point 5, the first characteristic is line 4 which has a negative slope separating regions a and c. Then, the path from point a to point c must have a negative slope, $-Z_1$, on the stress versus particle velocity plane. Since region c is free of crossing characteristics, there can be no discontinuities in pressure or particle velocity. Thus, the point defining the conditions in region c must be common to both lines drawn from points a and b on the stress versus particle velocity plane (Ref 13).

Assumptions

Various assumptions are essential in a spallation study. The first two assumptions necessary are that the material have the same properties in every direction from each point. These conditions are closely approximated since most metals are considered to be homogeneous, isotropic materials. The next three assumptions are the following: (1) the stress wave is plane, (2) the plane stress wave impinges on a plane free surface with normal incidence, and (3) only the plane stress component perpendicular to the surface is considered (Ref 3:2-1). The last two assumptions vital to a dynamic impact investigation are that one-dimensional strain be present and that the stress pulse generated by planar impact is representated by a square pulse.

Boundary Conditions

A shock wave is affected by abrupt changes in the physical properties of the medium through which it is traveling (Ref 24:2). The laws which govern the modification of the pulse as it crosses an interface between two materials are derived from the following two boundary conditions: (1) the stresses on the two sides of the boundary are equal, and (2) the particle velocities normal to the boundary are equal (Ref 24:15). The first condition results from the fundamental law of hydrostatic pressures and as long as normal incidence alone is considered this condition will hold for solids. The second condition is equivalent to specifying that the two media remain in constant contact at the boundary. These conditions hold for every point on the incident wave. The two equations which express these conditions are written as

$$\sigma_I + \sigma_R = \sigma_T \tag{5}$$

and

$$u_I + u_R = u_T \tag{6}$$

where σ_I, σ_R, σ_T, u_I, u_R, and u_T are the instantaneous values of stress and particle velocity, respectively for the incident, reflected and transmitted pulses, respectively. From conservation of momentum, it can be shown that

$$\sigma = \rho_o C u_p \tag{7}$$

where ρ_o and C are the density of the material and the velocity of propagation of the pulse, respectively. From Eq (7) it follows that

$$u_I = \frac{\sigma_I}{\rho_1 C_1}$$
$$u_R = \frac{\sigma_R}{-\rho_1 C_1} \tag{8}$$
$$u_T = \frac{\sigma_T}{\rho_2 C_2}$$

The subscripts denote the first and second media. Substituting Eq (8) into Eq (6)

$$\frac{\sigma_I}{\rho_1 C_1} - \frac{\sigma_R}{\rho_1 C_1} = \frac{\sigma_T}{\rho_2 C_2} \tag{9}$$

and solving Eqs (5) and (9) simultaneously, first for σ_T in terms of σ_I, then for σ_R in terms of σ_I, the two fundamental equations governing the distribution of stress at an abrupt change in media will be obtained:

$$\sigma_T = \frac{2\rho_2 C_2}{\rho_2 C_2 + \rho_1 C_1}\,\sigma_I \tag{10}$$

$$\sigma_R = \frac{\rho_2 C_2 - \rho_1 C_1}{\rho_2 C_2 + \rho_1 C_1}\,\sigma_I \tag{11}$$

When considering the transmission of a disturbance, a property of any medium is its specific acoustic impedance, Z, defined as the product of the density and the velocity of propagation of transient stresses (Ref 24:87). Then Eqs (10) and (11) can be written as

$$\sigma_T = \frac{2Z_2}{Z_2 + Z_1}\,\sigma_I \tag{12}$$

$$\sigma_R = \frac{Z_2 - Z_1}{Z_2 + Z_1} \sigma_I \qquad (13)$$

The problem of interest in this investigation is the process that occurs when a transient pulse traveling through a material encounters a free surface, where Z_2 is equal to zero. Applying this added condition to Eqs (12) and (13) results in

$$\sigma_T = 0 \qquad (14)$$

$$\sigma_R = -\sigma_I \qquad (15)$$

This says that there is zero stress at a free surface and that a reflected wave is opposite in nature from the incident wave. A compression wave is reflected as a tension or rarefaction wave. This rarefaction or tension wave unloads the target material to zero stress since it is equal to the compressive stress and opposite in sign (Ref 2:253).

Spalling

The phenomenon of spalling occurs when a compression wave in a solid is reflected at a free surface. At this surface the stress normal to the surface should be zero. Thus, the reflected wave is a tension wave which can interact with a compression wave moving through the same region as shown in Fig. 5. These two waves algebraically add according to the law of superposition; therefore, it

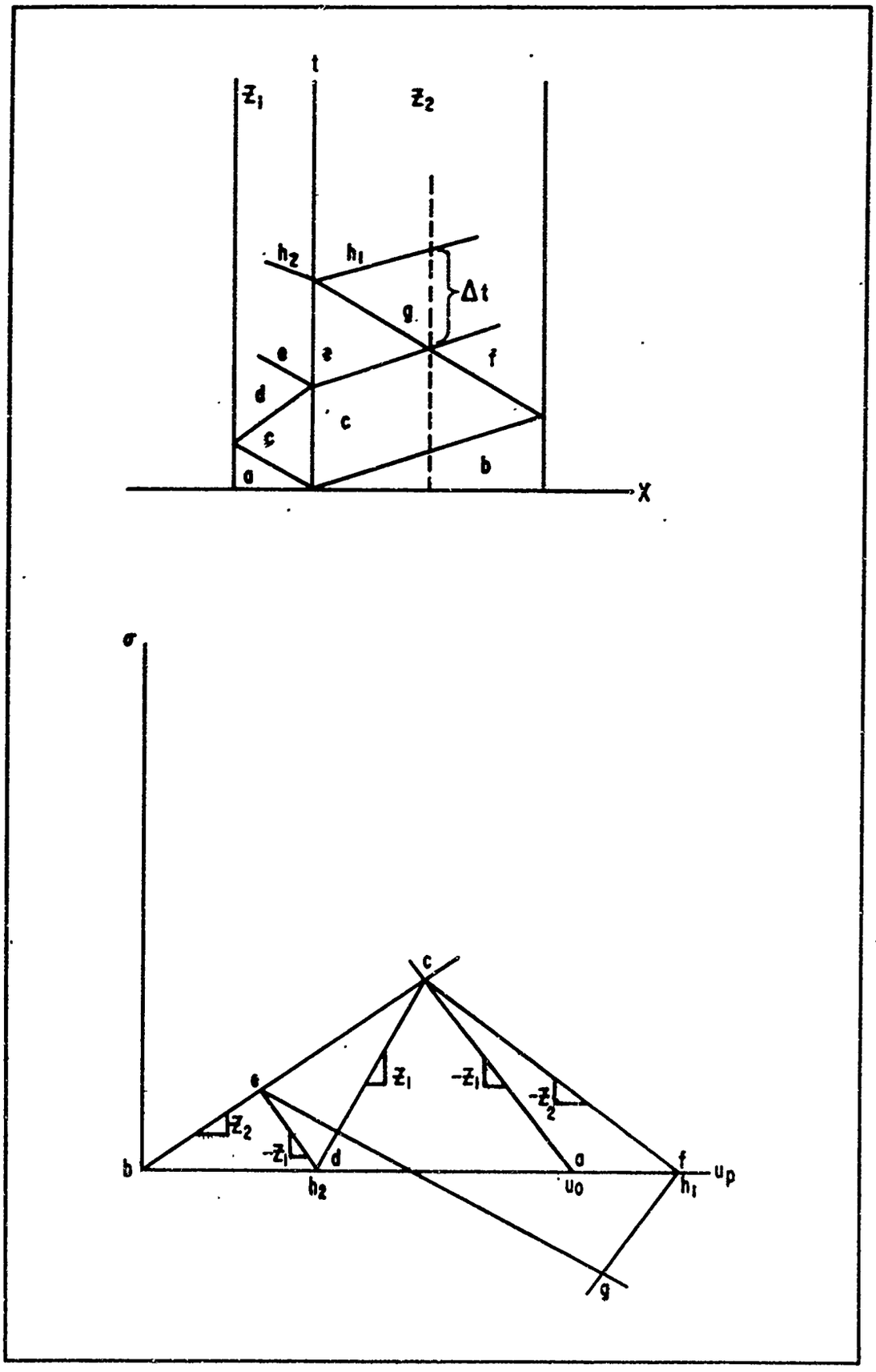

Fig. 5. Graphical Illustrations of the Occurrence of Spall

is possible for a net tension to be created in the target material. The tensile stresses can exceed the dynamic strength of the material at some distance from the surface. Then, fracture may occur at a surface parallel to the free surface and so a spall zone is formed. The impulse of the portion of the wave that is trapped in the spall gives a velocity to the spall, which flies off from the fracture surface (Ref 3:2-1). The wave interactions that lead to spalling can be seen in the time versus distance diagram of Fig. 5, and the tension created can be seen in the stress versus particle velocity diagram of Fig. 5.

Studies of the spalling of metal plates have shown that the two factors that have the greatest influence on spalling are the shape of the stress wave, and a critical normal fracture stress that is characteristic of the material acted upon (Ref 25:127). A knowledge of the distribution of stress as a function of time at all points in a material is important to establish a spall criterion; spall damage depends on peak stress and on pulse width. An equivalent distribution is that of flyer velocity as a function of flyer thickness. The critical normal fracture stress is defined as the mimimum, dynamic, tension stress required to rupture a material (Ref 24:36).

Spalling occurs in a short period of time (micro-second region), but it occurs in an orderly fashion. This phenomenon concerns large compressions followed by large tensions. Spalling is caused by stresses of very short

duration and of very large magnitude. The spall process is influenced by the pre-treatment given to the material by the compression wave, and it may be influenced by a temperature rise. For the purpose of studying the mechanism of spalling, it is essential to know that fracture starts at weak points in the material (Ref 3:1-10). The units pertinent to a dynamic, impact investigation are microseconds for time duration and kilobars for stresses. One kilobar is defined as 10^9 dynes per square centimeter.

Exploding Foils

The exploding foil assembly is a critical experimental requirement. An A exploding foil assembly is used to accelerate thin plates on the order of three to ten mils of Mylar. The experimental procedure section describes in detail the A assembly (Ref 9:221, 223). The pulse length of the shock wave produced in the material under investigation is primarily governed by the thickness and material of the flyer (Ref 9:227, 229). Therefore, by varying the thickness of the accelerated flyer plate, the pulse duration is varied; variation of the flyer velocity leads to variation in the peak pressure obtained (Ref 9:220). The thin plates are accelerated by producing a high-pressure, metallic vapor by rapid joule heating of an aluminum foil, enclosed in the exploding foil assembly, by a capacitor system (Ref 9:221) A uniform foil explosion enables the high-pressure gas to accelerate the thin,

flyer plate over a period of time as energy is transferred from the capacitor storage through the foil vapor into flyer kinetic energy (Ref 14:272). It is possible by varying the flyer velocity to describe the damage threshold of the material under study as a function of flyer thickness (Ref 9:221). The flyer velocity is the parameter of prime interest in this experiment since the initial particle velocity is of importance in the shock hydrodynamics. It is necessary to determine the flyer velocity for each experimental shot due to a variation of transfer efficiency.

III. Experimental Procedure

Introduction

All plate impact data were obtained at the Weapons Laboratory Pulse Power Facility. A capacitor bank was used to provide the energy needed to accelerate a flyer plate which impacted a target material; this process simulated X-ray induced shock waves. Thus, shock propagation resulted from planar impact with the geometry of the impact affecting the pulse shape and magnitude. The damage mechanism of spallation was of prime concern. The velocity and thickness of the flyer are important parameters since they can be transformed into peak pressure and pulse width respectively in the shock wave.

This section will be concerned with the experimental equipment and experimental procedure. The capacitor bank will be discussed along with the impact configuration; the exploding foil assembly that produces the flyer plate for impaction on the target plate will be described. After discharging the capacitor bank, it is possible to obtain a record of the flyer flight and impact by photographic techniques. The experimental arrangement can be seen in Fig. 6. Also included in this section will be a description of the equipment employed for obtaining the flyer velocity. Macroscopic and microscopic analyses performed after impact are also important. Finally, a preliminary vacuum, impact study is described.

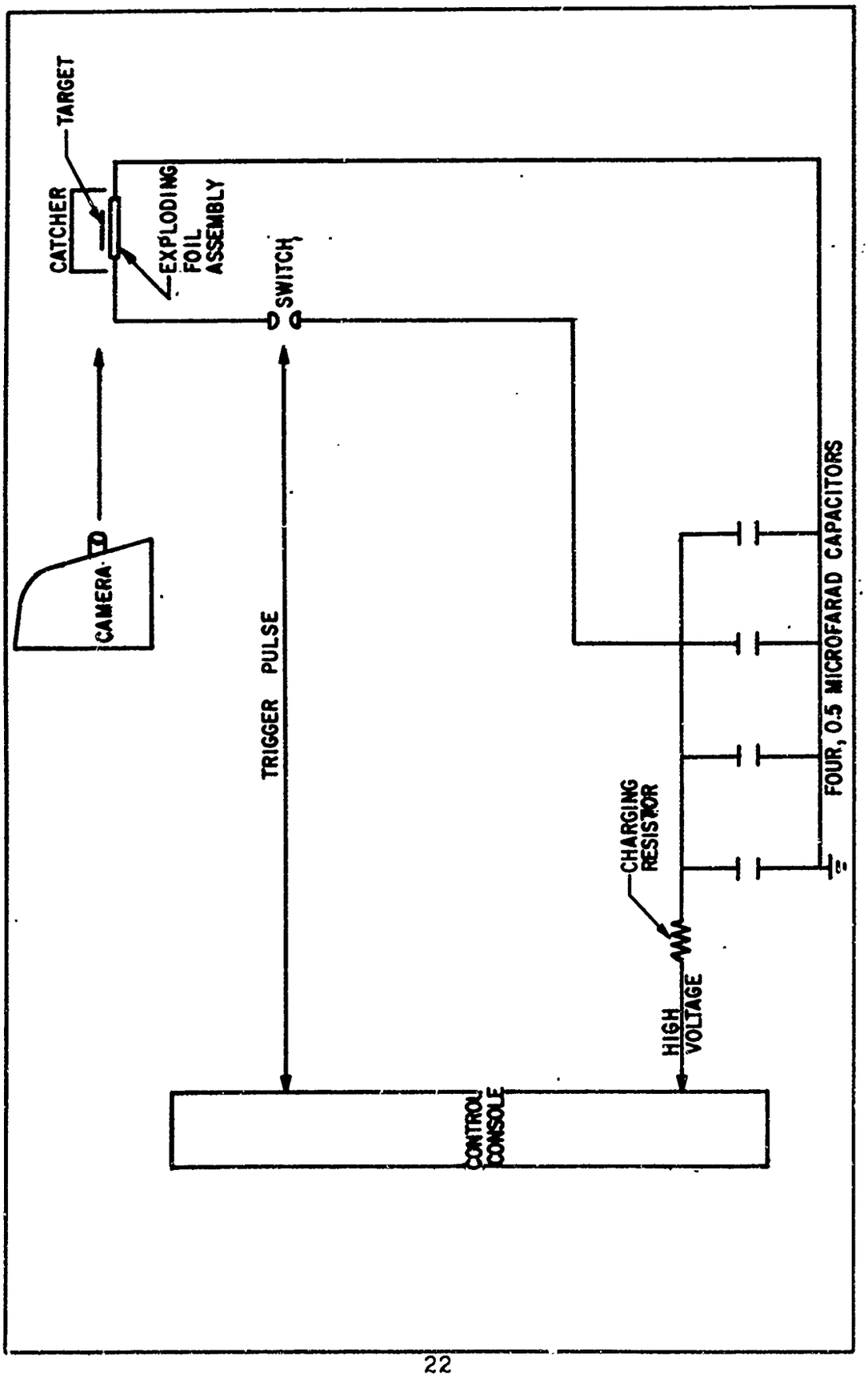

Fig. 6. Overall Equipment Diagram

Capacitor Storage System

A detailed description of the equipment available at the Pulse Power Facility can be found in a report by Wunsch, Soapes, and Guenther (Ref 30); this discussion is a summary of the techniques that they have developed.

The capacitor storage system was arranged geometrically in a square consisting of four, 0.5 microfarad Axel Capacitors which were electrically connected in parallel. The exterior of the capacitor bank was ground with the metallic portions made from aluminum. The high-voltage plate was located in the interior of the bank, and the bank was filled with a high-grade transformer oil in order to prevent electrical breakdown, thereby allowing closer spacing between high-voltage parts.

The capacitors were charged through a three megaohm resistor by a commercial power supply. A charging current of about 3.5 milliamperes was usually obtained. The capacitor bank had a total capacitance of two microfarads and had a capability of firing 125 kilovolts and dumping up to 16,000 joules. The dumptime was 1.5 microseconds with a ringing frequency of 1/3 megacycle.

The capacitor storage system was discharged by a triggered spark gap switch through a thyratron circuit using a pulse transformer to produce a triggering pulse. The spark gap was pressurized from atmospheric pressure up to 60 psi to hold off higher voltages and insure the capability of

discharging the bank over a range of voltages obtaining reliable triggering.

Flyer and Target

The flyer material used was Mylar, and the samples were 3.0 by 3.5 inches with a tolerance of 0.015 inch. The Mylar thickness varied depending on the particular need; the thicknesses used in this study were 3, 5, 7.5, and 10 mil (0.001 inch = 1 mil) all with a tolerance of 0.1 mil. The Mylar flyers were obtained preassembled in an exploding foil assembly.

The target material used was a structural alloy, 6061-T6 aluminum; a complete alloy designation can be found in Appendix B. The target samples were cut from sheet stock of 6061-T6 Al, and in all cases the samples were 1.75 $\pm$ 0.05 inches square with a thickness which remained constant throughout the investigation. The thickness was 0.032 inch with a tolerance of $\pm$ 0.003 inch. All experimental shots used samples from the same sheet in an attempt to insure consistency of material properties.

Exploding Foil Assembly

An exploding foil assembly or transducer load was necessary in order to accelerate thin Mylar flyers to impact on the aluminum target. Each experimental shot performed for this study required a new transducer load; the nomenclature for the transducer load used was A 0.25 Al (3/2 X 3/2) MYLAR, referred to as an A load. The type of

load was A, 0.25 Al refers to the thickness in mils of the aluminum foil used, and 3/2 X 3/2 is the size in inches of Mylar that will rip out upon vaporization of the aluminum foil.

The elements of the exploding foil assembly used in this experiment were a back-up block, copper electrodes, an aluminum foil, a Mylar sheet, and a barrel, which was made up of two sections. The construction of an assembly differs according to the limitations placed on the parameters in question, and various of these assemblies are discussed in several references (Ref 6, 9, and 30). A block diagram of the A assembly is shown in Fig. 7, and a photograph of the A assembly is shown in Fig. 8. Appendix C consists of figures of each of the elements in the A exploding foil assembly.

The back-up block was made of plexiglass, and the block was three inches square and a half inch thick. The function of the back-up block was to confine the explosion; an increase of shock block thickness increases flyer velocity (Ref 9:225). For this investigation, however, a half-inch shock block thickness was satisfactory. The back-up block had two grooves on two opposite sides; the grooves were milled to 0.005 $\pm$ 0.0005 inch deep and were centered 1 1/2 inches along opposite sides. The grooves ran 3/4 inch towards the middle of the square side of the block. Copper electrodes, 0.005 inch thick, were then glued into the grooves on the back-up block using Eastman

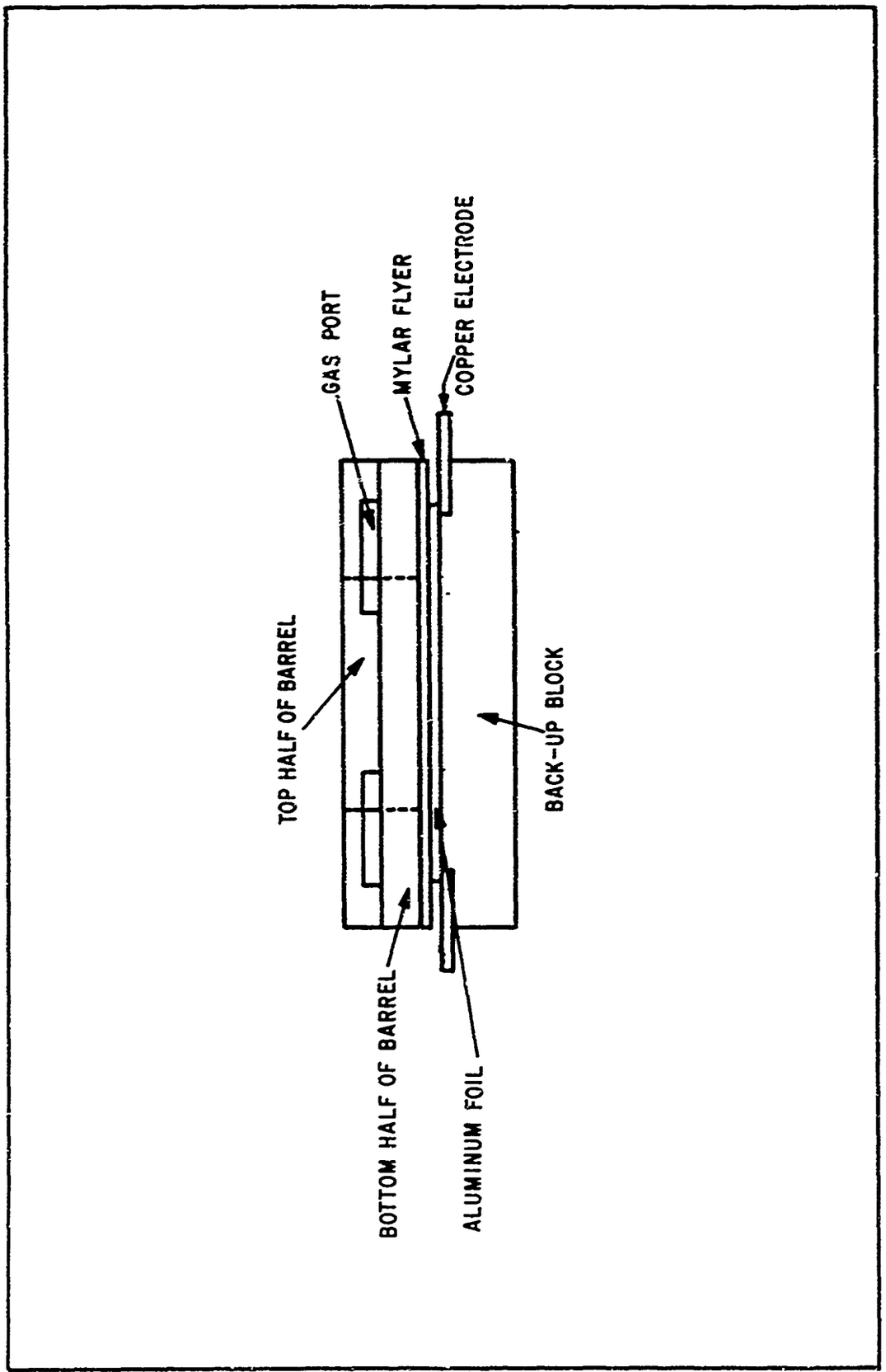

Fig. 7. Diagram of A Exploding Foil Assembly

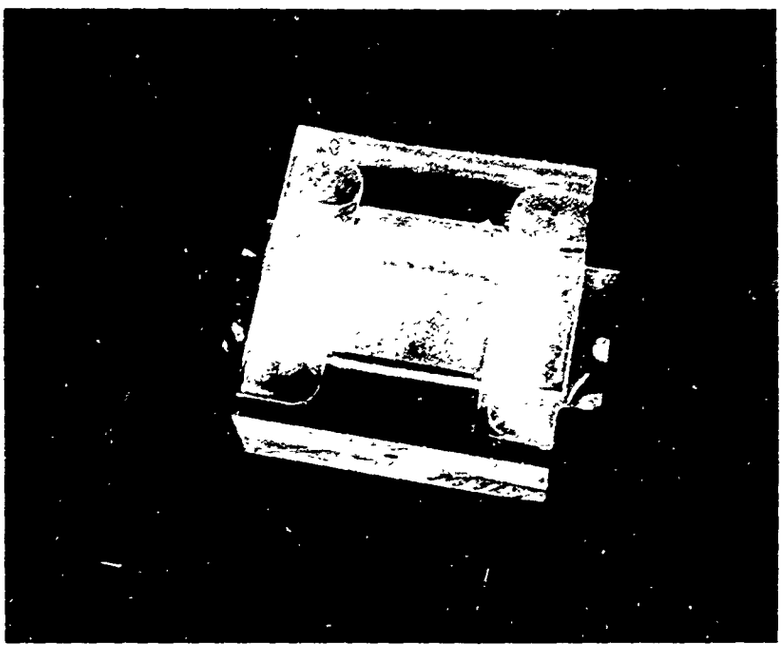

Fig. 8. Photograph of A Exploding Foil Assembly

910 adhesive; they were fitted into place in the grooves with a portion of the electrodes extending out past the block. This was true because the electrodes were 1 1/2 inches square. In other words, approximately half of each electrode protruded from the back-up block. This permits joining the exploding foil assembly to the capacitor bank system. Next, a 0.25 mil aluminum foil was placed in line with the copper electrodes but centered in the back-up block. Since the foil was 1 3/4 by 1 1/2 inches, the longer dimension overlapped equally (1/8 inch) in both directions over the copper electrodes. A thin coat of conducting silver was spread between the electrodes and the foil. A sheet of Mylar, 3 by 3 1/2 inches, was glued over this entire block arrangement. The long dimension was assembled 90° from the copper electrodes producing a half inch overlap of Mylar on this side. This half inch may be used to verify flyer thickness. The bottom half of the barrel was then glued to the assembly. This part of the barrel was also made from plexiglass; it was a block 1/4 inch thick and 3 inches square. But it had a 1 1/2 inch square section cut out in the center which determined the size of flyer. The top half of the barrel was then glued to the bottom half. The top half of the barrel was similar to the bottom half except that the top half had gas ports, directly above the copper electrodes. The gas ports aid in viewing the Mylar flyer during flight by directing gas flow away from the viewing area (Ref 9:223). It should be

pointed out that the tolerance of the parts of the assembly was 1/64 inch unless specified otherwise above.

Plate Impact

Before the exploding foil assembly was placed in its impact configuration, it was heated under a lamp for approximately 15 minutes to eliminate air bubbles between the Mylar and aluminum foil. It was believed that this treatment enabled the aluminum foil to vaporize more uniformly, therefore, improving planarity.

The thin flyer was accelerated above the top of the bank and was impacted upon the target material. The exploding foil assembly was joined to the capacitor bank by clamping the copper electrodes of the assembly to the electrodes of the bank. The capacitor bank was discharged through a control console. All experimental runs were performed at room temperature and pressure.

With the above arrangement, the discharging of the capacitor bank caused the aluminum foil to vaporize producing a high pressure, aluminum vapor. This vapor ripped out a section of Mylar the area of which was determined by the dimensions of the barrel — 1 1/2 inches square. The Mylar was accelerated at a high velocity that was determined by the voltage, the efficiency of discharge, and the thickness of the aluminum and Mylar foils. For this particular study the aluminum foil thickness was a constant since only A loads were used. Transfer efficiency was defined as

the ratio of flyer kinetic energy to the initially stored, electrical energy. The flyer velocity required for the target spall threshold determined the range of bank voltages and the particular aluminum foil needed. For all experimental shots, the transfer efficiency ranged from 20 to 69 percent. Oscilloscope traces were obtained for each shot of the current change through the aluminum foil. The current waveform (di/dt) was a good indicator of the efficiency of energy transfer (Ref 9:231, 232).

The Mylar flyer traveled approximately two centimeters before impacting the aluminum target that was isolated above the foil assembly by a bracket arrangement. An air gap was present between the load and the target; a constant distance was maintained for all experimental shots to keep the same volume of air in the gap. The target was positioned far enough from the exploding foil assembly so that there was insufficient time for the target to be disturbed before the impact of the flyer (Ref 21:5). A more important consideration was that the separation had to be sufficiently great for the flyer to attain a terminal velocity (Ref 21:15). After each experimental shot, the flight of the target was terminated by a padded box that had been placed over the experimental area of the capacitor bank. A photograph showing the exploding foil assembly, the 6061-T6 Al target, and the testing area of the capacitor bank before firing may be seen in Fig. 9.

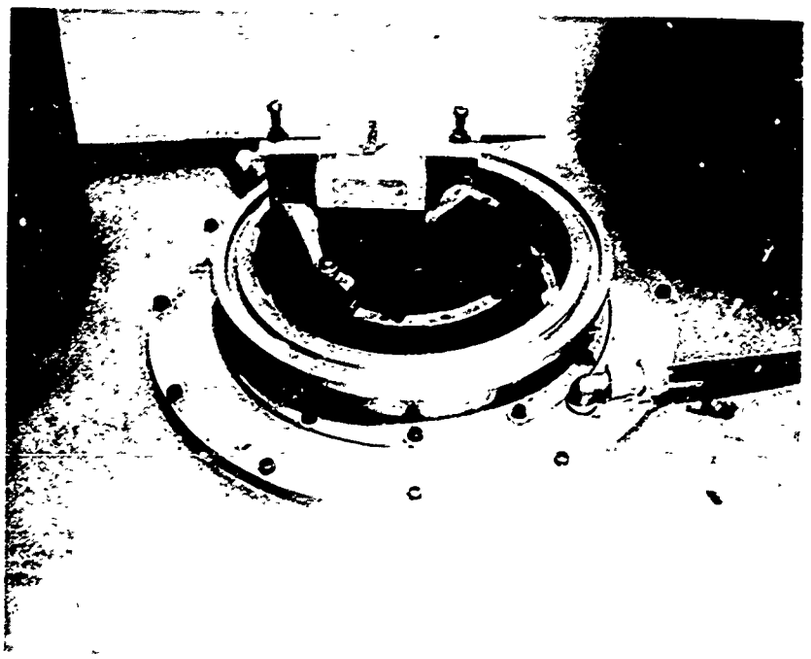

Fig. 9. Impact Configuration

The preceding arrangement was used for this experimental study, but it is possible by changing exploding foil assembly parameters to perform different experiments. Thus, by varying the voltage on the bank and by changing assembly parameters, one is able to achieve a reasonable flyer velocity range (Ref 9:227).

Spall Threshold

For each particular flyer used the voltage which caused the 6061-T6 Al target to spall was found. Then the voltage was varied on both sides of this threshold voltage by small increments to obtain numerous velocity points near the damage - no damage threshold point. By adjusting the initial voltage on the energy storage capacitors, it was then possible to vary the flyer velocity. It was possible to accelerate the thinner Mylar flyers to higher velocities (Ref 9:226). This procedure was repeated with each different flyer (3, 5, 7.5 or 10 mil) used, but in all cases the thickness of the target (32 mil) was kept constant.

Framing Camera

A Beckman and Whitley, Model 189, High-Speed Framing Camera was used to photograph the flyer motion. It was possible to obtain 25 frames with this camera with framing rates as high as 4.5 million frames per second. The controls for the camera were also on the control console used for the capacitor bank.

A report by Wunsch and Guenther (Ref 29) describes in detail the framing camera used in this investigation. High-speed framing cameras make use of rotating mirrors and field stops, and they exhibit a changing field of view and of frame size as the mirror rotates. The use of the frame edge as a reference line requires that the magnitude of these effects be known. The determination of the flyer velocity using the framing camera required measuring on the film the distance the flyer had moved from the reference line. The best way to make the velocity measurements was by measuring movement with respect to the frame edge. Therefore, to make velocity measurements using the frame edge as a reference line, one must make corrections for the change in frame size and the shift in the field of view.

The films obtained from the Model 189 camera were processed at the facility using a Recordak Prostar Film Processor. Less than five minutes was required to process each film. Each shot film was examined for planarity with the aid of a film viewer. After the planarity was determined, the average velocity of the flyer was also determined from the film.

Velocity Determination

The velocity of the Mylar flyers was determined from the high-speed photographs obtained for each experimental determination. The 35 millimeter negative film was read on a Richardson Film Reader which has the capability of viewing

the displacement of the flyer between frames. The techniques necessary to operate the reader are discussed in the report by Weis, Sanchez, and Guenther (Ref 28:2).

Damage Determination

After a target was shocked, macroscopic and microscopic investigations were conducted on the recovered target. To insure one dimensionality only the center of the specimen was considered. If spall was not visible, the sample was examined in the metallurgy laboratory.

Only the samples from the shots with the best planarity were checked for damage microscopically at the metallurgy laboratory. Samples were sectioned as depicted in Fig. 10. The center sections obtained from the impacted targets were mounted and polished, then viewed microscopically for damage. The sample was investigated for damage only at the center of the sample to eliminate edge effects. If no damage was observed, the sample was etched, then viewed for damage again. A detailed narrative of the metallurgical procedures required can be found in Appendix D.

Vacuum Shots

Preliminary vacuum shots were conducted. The same experimental geometry as the air shots was employed except that the impact configuration was enclosed by a bell jar, and this enclosure was evacuated to approximately 10^{-6} mm Hg. This eliminated the air cushion from affecting the

flyer. All of the techniques described previously were also used for the vacuum shots.

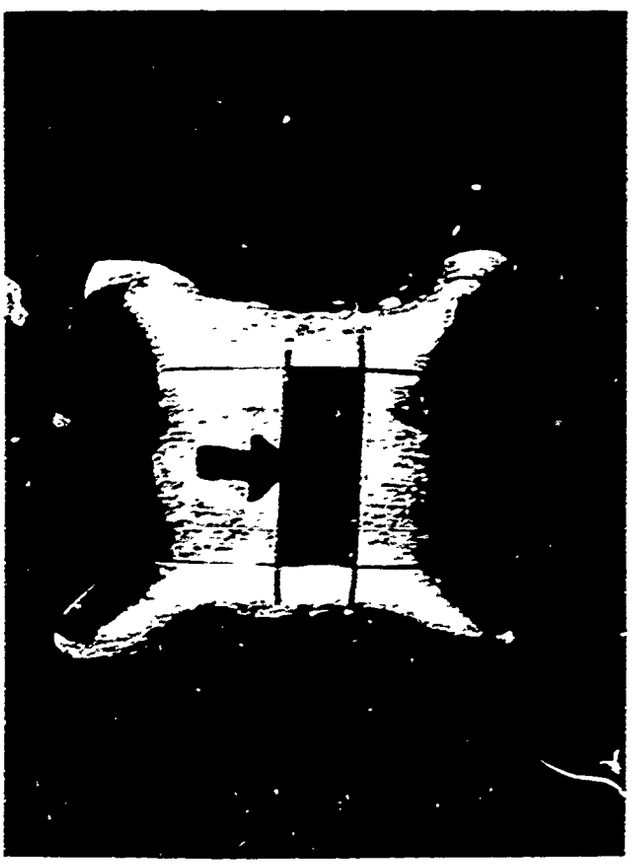

Fig. 10. Sectioned 6061-T6 Aluminum Target

IV. Data Analysis

Equations-of-State

Mylar was chosen as the flyer material because it has been considered to be the best projectile for an exploding foil investigation when high pressures over a short duration are required (Ref 9:244). Mylar is considered an excellent flyer; however, its equation-of-state is not well known. Inability to obtain Mylar sheets thicker than 14 mil has prevented obtaining a complete equation-of-state for Mylar (Ref 9:244). The data presently available at the AF Weapons Laboratory are not known well enough above 16 kilobars, but J. R. Penning of the Boeing Company has recently obtained data for Mylar valid up to 30 kilobars (Ref 20). Nevertheless, the equation-of-state of Mylar will have to be completely determined before a complete analysis is possible.

The target material, 6061-T6 aluminum, was chosen because its Hugonoit equation-of-state was readily available. Another important factor contributing to its selection was the availability of shock impact data for this particular alloy. This was desirable since it could provide a comparison if necessary.

Impact Geometry

Important factors are present in the design of a flying plate experiment. The target to flyer thickness ratio must be large enough to prevent the catch-up of a rarefaction wave, but this thickness ratio must not be too large such that it disturbs the spall region near the axis. After a plate thickness ratio is determined, it should be kept constant to insure that the pulse shape remains constant.

If the ratio of plate thicknesses is too small, then a rarefaction from the free surface of the flyer plate will overtake the collision-produced shock, before this shock reaches the free surface of the target plate (Ref 15:173). Clearly, this minimum ratio of thicknesses will vary according to the particular investigation concerned. This minimum required ratio may be obtained graphically on the time-distance plane. The shock wave propagation with time will indicate the minimum plate thickness necessary in this case for a Mylar flyer and a 6061-T6 aluminum target. The design of this experiment using 3, 5, 7.5, and 10 mil flyers each impacting a 32 mil target took into account the rarefaction wave catch-up point.

If the ratio of plate thicknesses is too large, the edge effects may influence the central region of the target. A check to insure one-dimensional strain can be accomplished on a time versus distance plot, Fig. 11 (Ref 4). The minimum distance that the wave must travel in the target material

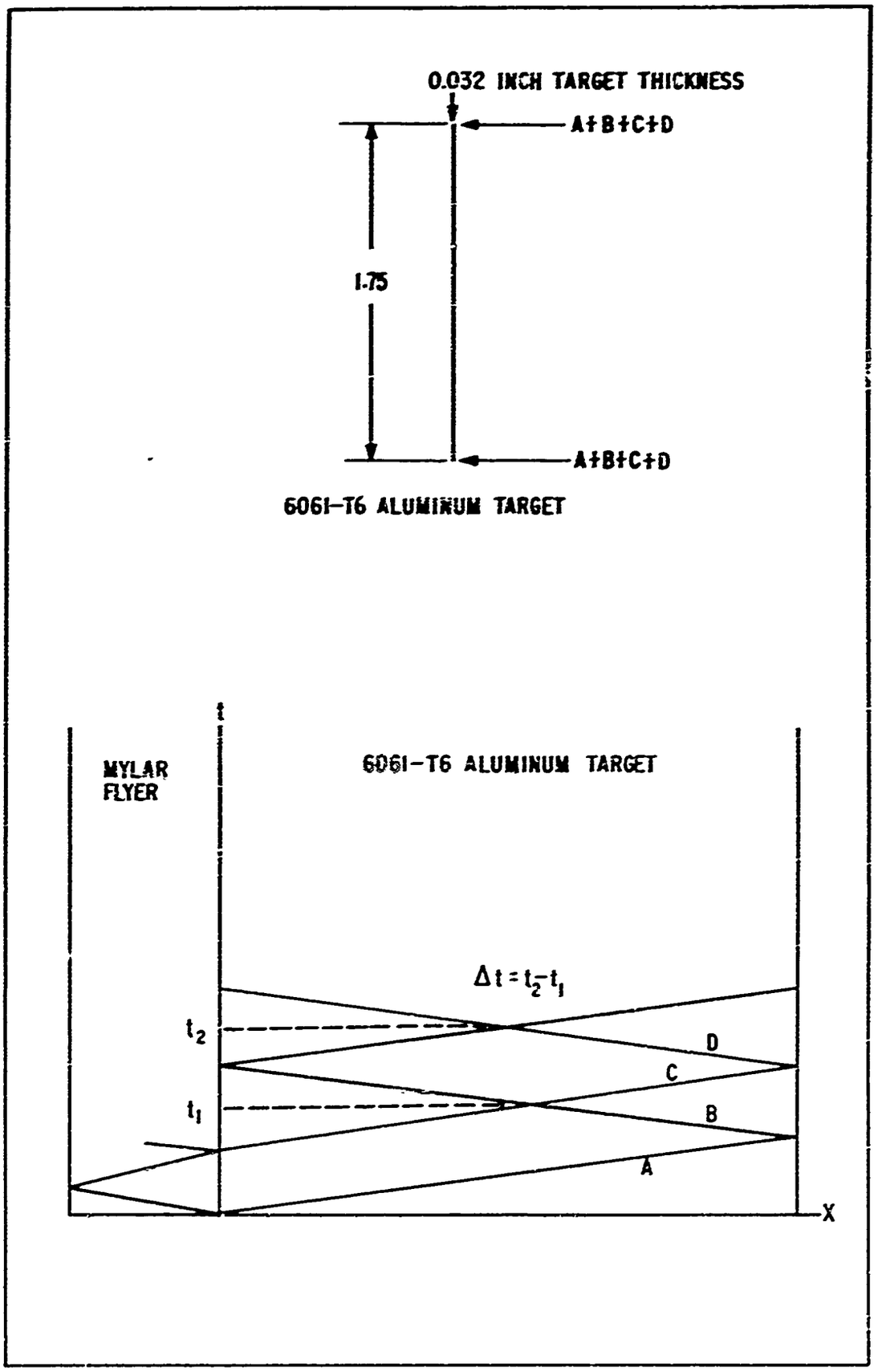

Fig. 11. Determination of the Influence of Edge Effects

to allow for possible spallation is equal to (A + B + C + D). As long as the lateral dimensions of the target are much larger than its thickness, the distance (A + B + C + D) will be insignificant. For example, the greatest that (A + B + C + D) can be for this investigation is approximately 0.075 inch which is truly insignificant compared to the lateral dimensions of the target, 1.75 inches square. Thus, the impact will be completed before the effects of the edge can be experienced.

Since this experiment did not allow for a constant plate thickness ratio, the data obtained was pulse shape dependent. This failure to scale the target causes differences in pulse durations (Ref 6:985). For this experiment the time duration was such that the plate thicknesses used would not significantly alter the pulse shape. It can be said that the pulse shape remained square. The pulse shape of the thinnest flyer, 3 mil, would be most influenced.

Planarity

The dependability of many of the experimental shots was limited by the amount of tilt present between the flyer and target at impact. This question of planarity required a criterion to specify the degree of departure from planar impact. Such a criterion was necessary in order to increase the accuracy of this experiment. The literature cites in many cases the use of pins to measure the tilt or planarity, but this method usually causes an error in the

velocity determination. The most feasible course was to formulate a criterion using the 35 millimeter film record obtained with the high-speed camera. This film was a record of the flyer flight and impact; therefore, the films could easily be observed on a film viewer for flyer planarity at impact. It was important to formulate a criterion and to apply it consistently on each experimental shot. The planarity criterion was entirely arbitrary, and it was based on the best planarity being the flattest. Planarity was divided into four classes which are the following: P-1, P-2, P-3 and P-4. Planarity-one or P-1 was the flattest impact observed on the film. Fig. 12 shows photographs which are typical examples of three of the four classes of planarity. The four classes of planarity were assigned because all shots seemed to fall into one of the four levels. The worst planarity, P-4, is not represented in Fig. 12, but it was a level with more curvature at impact than P-3.

Damage Classification

A criterion to describe the damage after the flyer-target impact was essential; the damage of primary interest in this investigation was that of spall. The damage criterion used to classify the recovered 6061-T6 aluminum targets was based on whether the damage was external or internal. It was necessary to apply this criterion consistently in classifying each recovered specimen.

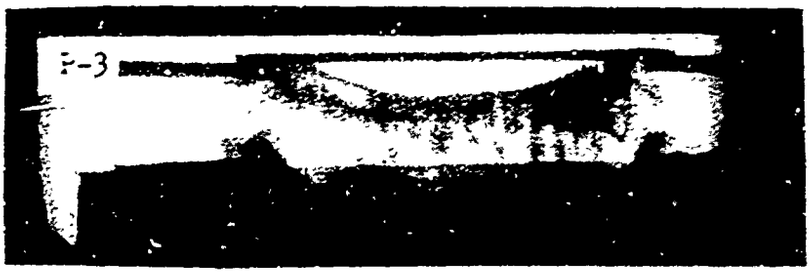

Fig. 12. Examples of Planarity, P-1, P-2, and P-3

To insure one-dimensionality, it was expedient to consider only the center region of the impacted samples. After preliminary investigations, it became apparent that further analyses would have to be limited to the experimental runs that were classified as P-1. The scatter of data was too great if the other planarities were considered.

Recovered samples of 6061-T6 aluminum were considered to have spalled only if the spall was visible, otherwise the sample was examined at the metallurgical laboratory. A photograph of a spall sample can be seen in Fig. 13. At the metallurgical laboratory center sections were obtained from the impacted targets and then mounted, polished, and viewed microscopically for possible internal spall. Spall found in this manner was termed incipient spall. Two examples of incipient spall can be seen in Fig. 14 and Fig. 15. If none was observed, the specimen was re-polished and etched then viewed for damage again. When incipient spall was observed for this experimental set-up, it occurred in a single spall zone. In most cases, incipient spall was found after polishing, therefore, not requiring etching. If no damage was observed, the impacted target was classified as a no spall specimen. Therefore, recovered samples could be classified into one of three classes —— spall, incipient spall, or no spall.

This concept of classifying the damage is not a new one, and the terminology is certainly not new. It is only that these classifications have been defined to mean

Fig. 13. Spalled 6061-T6 Aluminum Target

Fig. 14. Incipient Spall in 6061-T6 Aluminum Target(Top Edge)

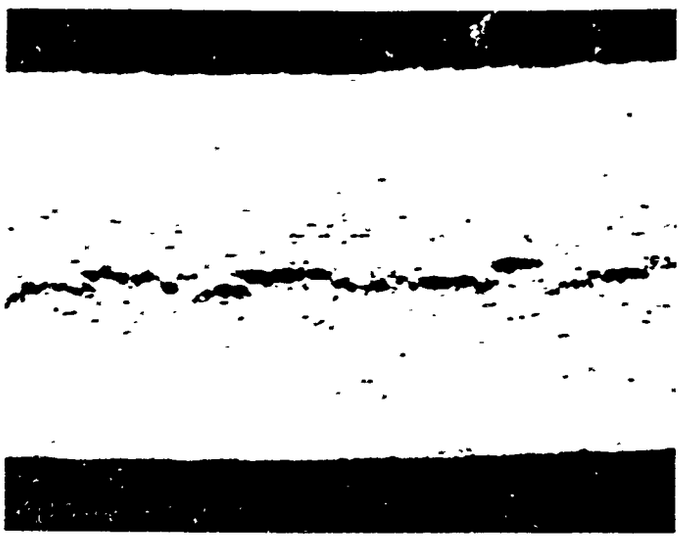

Fig. 15. Photomicrograph (50X) of Incipient Spall

different stages in the spall process depending on the particular investigator. As a result, it is sometimes difficult to correlate similar results.

Flyer Velocity

It was apparent beforehand that the determination of the flyer velocity for shots classified as P-3 or P-4 would be of little value. Afterwards, it was also resolved to reject P-2 shots because an unacceptable scatter of data resulted. The importance of obtaining the best possible flyer velocity for the P-1 shots was evident.

Flyer velocities were calculated from the shot film records that were read using a Richardson Film Reader. The velocity was computed by dividing the difference in displacement between consecutive frames by the time interval between them. Displacement was measured at the center of the impacted sample. The velocity at several points was determined to obtain an average flyer velocity. Personnel at the AF Weapons Laboratory Pulse Power Facility have developed computer programs that determine the flyer velocity and its error (Ref 28:3). The programs account for camera corrections, and they reject spurious data employing the method of least square. The error involved in the calculation of the average flyer velocity was five per cent for P-1 data.

Graphical Representation

The experimental data is presented, Fig. 16, in a plot of flyer velocity versus flyer thickness. The third parameter depicted in this representation is that of damage classification. It must be emphasized that these data are only for the best planarity shots, those that were P-1. The area above the curve is the damage area for the 6061-T6 aluminum; damage is considered to be both spall and incipient spall. The area below the curve is the no damage or no spall area for the target material. A least squares fit was applied to this experimentally determined exponential curve, and the following equation was obtained:

$$V = C_1 \exp(-C_2 M) \qquad (16)$$

where $C_1 = 3.326$

$C_2 = 0.06505$

V = flyer velocity in mm/usec

M = flyer thickness in mils

The above equation can be used to find the values of flyer velocity for different flyer thicknesses at the point of separation between damage and no damage. This point of separation between damage and no damage can be defined as the spall threshold of the material. The flyer velocity was calculated using Eq (16) for the flyer thicknesses used in this investigation and the velocities calculated were within the five per cent error associated with the ex-

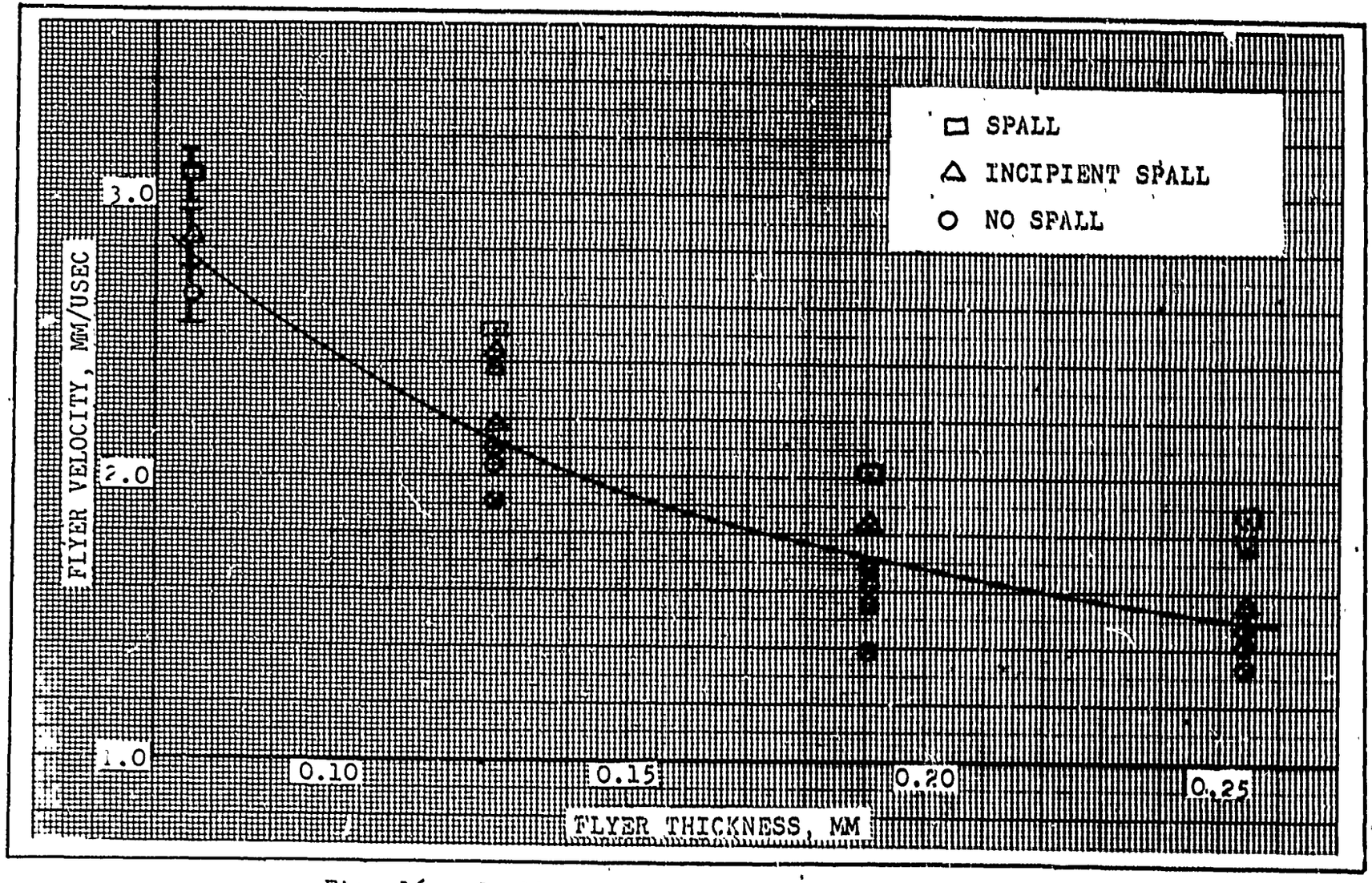

Fig. 16. Spall Threshold of 6061-T6 Aluminum

perimental determination of the average velocity.

The initial velocity or flyer velocity can easily be converted to the peak pressure reached upon impact providing that the Hugonoits of the flyer and of the target are known. First, the target Hugonoit is plotted on the stress-particle velocity plane starting at the origin since the target is initially at rest and unstressed. Next, the flyer Hugonoit is also plotted on the stress versus particle velocity plane with initial conditions of the flyer unstressed but at initial velocity. The flyer Hugonoit is extended until it intersects the target Hugonoit, and this intersection defines the impact or peak pressure and the impact velocity. The intersection dictates the impact pressure and velocity since it is the only point common to the material Hugonoits; therefore, the intersection satisfys the boundary conditions that must be met. The boundary conditions being that the stress and particle velocity be equal at the impact surface. This process is illustrated in Fig. 17 for several initial velocities. The flyer velocity was not converted to impact pressure because of the uncertainty existing in the Mylar Hugonoit. Until the Mylar Hugonoit is completely determined, it is better to present the data with the flyer velocity.

The tension pulse duration is a function of the flyer thickness. The thickness of the flyer can also readily be transformed graphically to pulse duration. This can be accomplished on the time-distance plane as can be seen in

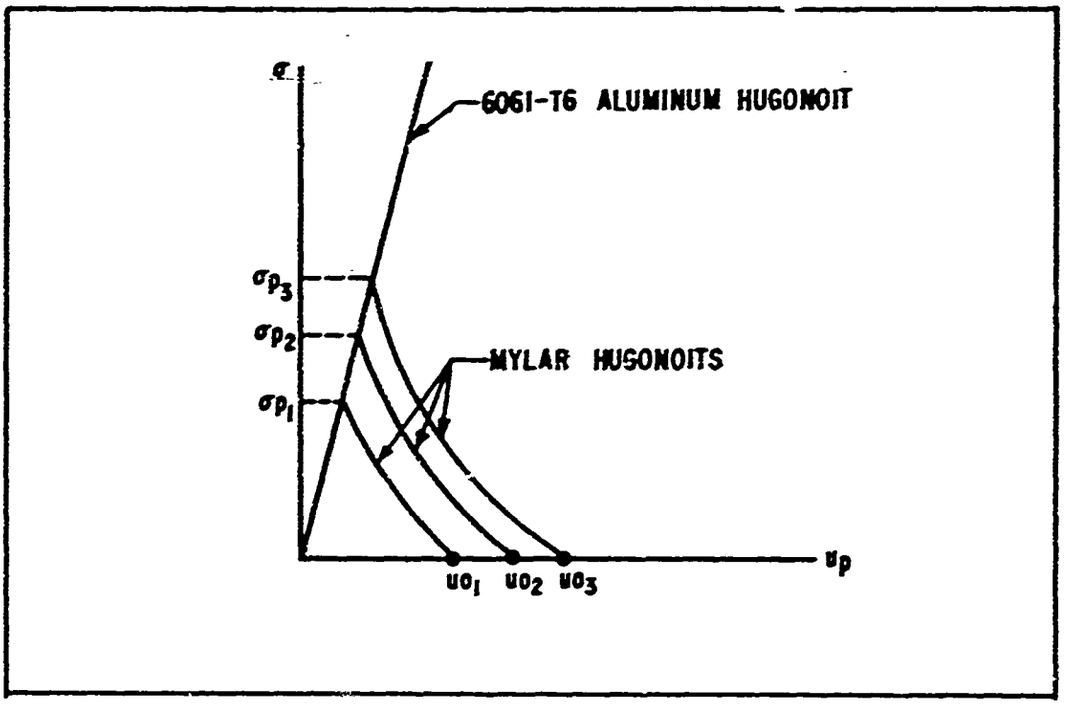

Fig. 17. Conversion of Initial Particle Velocity to Peak Impact Stress

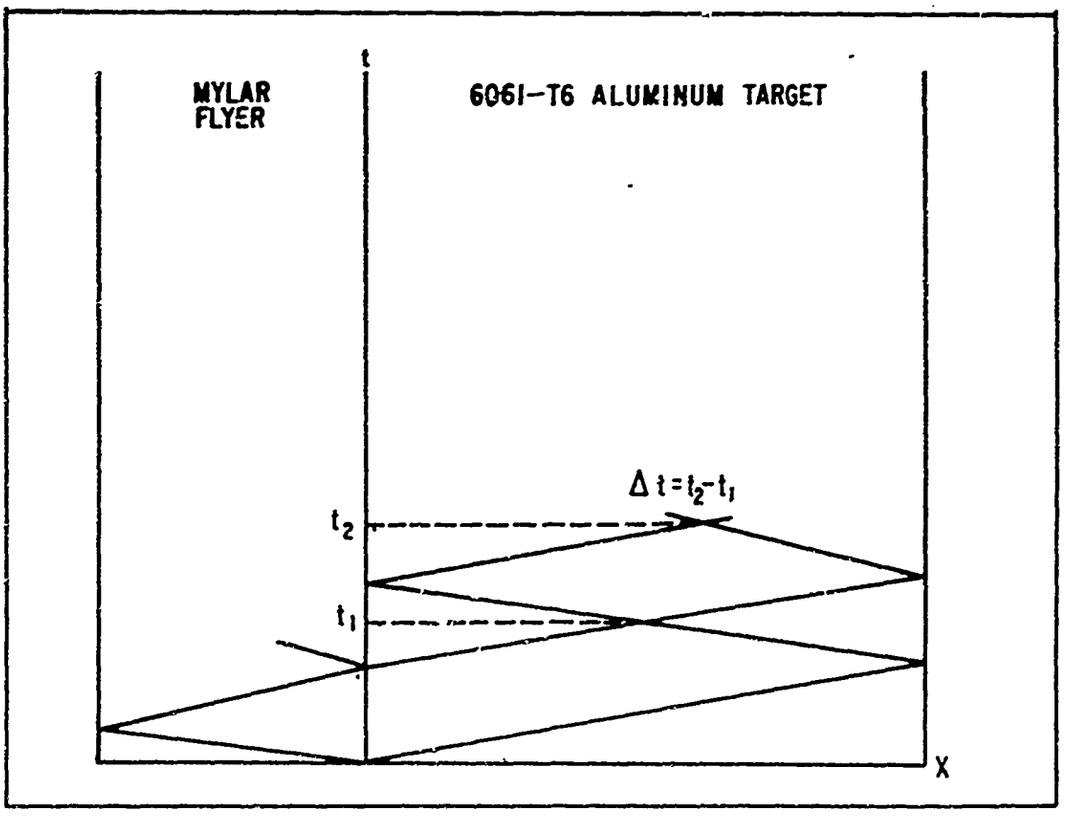

Fig. 18. Conversion of Flyer Thickness to Pulse Duration

Fig. 18. From this figure, it can be seen that the pulse duration is $t_2 - t_1$. When a conversion of flyer velocity to impact pressure is practical, it will then be useful to present a spall threshold curve with impact pressure and pulse duration.

Spall Measurements

An attempt was made to correlate the experimental, incipient spall locations with each flyer thickness. Photomicrographs were obtained for the incipient spall samples at 25X then incipient spall measurements were obtained from these photomicrographs. These measurements were approximate since it was difficult to define the spall plane. Once the spall plane was assigned then an additional error was introduced in the measurements, $\pm$ 0.05 cm. The total maximum error in these incipient spall measurements was 15 per cent. Generally, it could be said that as the flyer thickness was decreased, the spall plane was formed closer to the free surface. The exact spall location is very difficult to resolve with great precision experimentally since spall generally occurs over a region in the material rather than at a discrete plane (Ref 6:993).

Microscopic Analyses

The microstructure of the specimens that had been classified as incipient spall was examined. Since there were numerous samples in various stages of incipient spall, it became possible to try and observe how these spalls were

propagated. The metallurgical analyses were performed at the AF Weapons Laboratory by John E. Cooney. Early in this investigation, he observed that cracking seemed to start in the inclusions present in the 6061-T6 aluminum. It was noticed that in some samples only the inclusions seemed to have cracked and in others cracks seemed to run from inclusion to inclusion. After further metallurgical examination of the specimens, he was able to show that the more brittle inclusions cracked then the damage propagated from inclusion to inclusion through the matrix material. This can be seen in the photomicrographs presented in Fig. 19 and Fig. 20.

It is believed that impulsive loading increases the hardness of a material subjected to shock waves (Ref 1: 197). A hardness survey for 6061-T6 aluminum was performed by Cooney. A detailed narrative of the analysis is in Appendix D.

Air Cushion

This investigation was performed at room temperature and pressure, but an air gap was present for each experimental shot maintaining approximately a two centimeter separation. Since the variation in flyer thickness used was not great, it was believed that keeping the amount of air between the load and target approximately constant would have approximately the same effect on each of the different flyers. They would all experience approximately

Fig. 19. Photomicrographs (1000X) of Cracked Inclusions

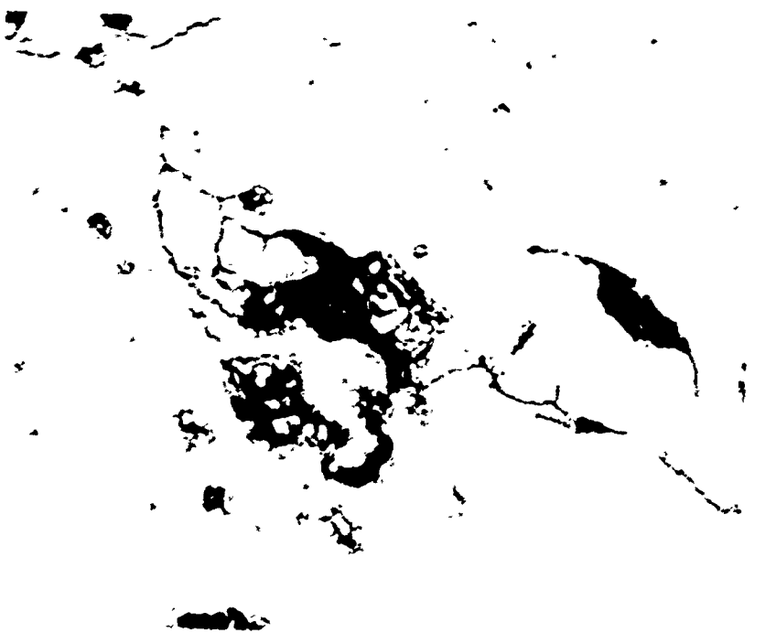

Fig. 20. Photomicrograph (1000X) of Crack Propagation

the same amount of air cushioning before impact. After the air shots had been completed, it was decided because of the various publications concerning air cushioning of thin flyers to investigate this effect. Only a preliminary study was accomplished, and it revealed that a more extensive study is required. For a 5 mil flyer, it was found that the vacuum spall threshold was 25 per cent lower than that in air. This percentage may be even greater, but it was not possible to obtain an exact comparison because the operational capacitor bank spark gap reached its lower voltage limit.

Since the air is progressively compressed as the flyer plate approaches the target plate, it might be expected that the wave profile induced in the target plate will differ from that induced in the absence of air (Ref 11:62). The most important effect of air is in altering the wave profile. The magnitude of the effect of an air cushion depends on the driver plate thickness. For very thin flyer plates, the peak pressure at the interface will be attenuated (Ref 11:76). A possible solution to the problem of air cushioning could be reached by decreasing the thickness of the air gap; however, in the plate impact method, it is necessary to provide a suitable gap to allow the flyer to accelerate to essentially constant velocity, reach a steady state (Ref 12:482).

The effect of an air cushion has been determined for Plexiglass (Ref 16:19, Ref 21:19). A flyer free run dis-

tance of 1/16 inch was used both for a normal atmosphere environment and a vacuum environment. For flyers greater than 30 mil, the Plexiglass spall threshold did not vary either in air or vacuum. For flyers varying from 10 to 30 mil, there was not too great a difference in spall threshold measurements, about 0.01 centimeter per microsecond. The effect of an air cushion becomes critical for Plexiglass flyers less than 10 mil. These Plexiglass data serve as a strong indication that a similar study should be performed using Mylar. The Plexiglass data can not be directly correlated with the Mylar data because of the differences in experimental techniques. The densities of the two plastics are different, and a free run distance of two centimeters was used in this experimental investigation.

Guenther states that once the mass of the flyer exceeds the mass of the air separating the flyer and target, air cushioning ceases to be a major problem. In general, this effect becomes noticeable for flyers thinner than 1/32 to 1/16 inch and is, therefore, important for Mylar accelerations, where a flyer twice as fast in air as one in vacuum may be required to produce damage (Ref 9:235).

Sandia Corporation attempted to explain variations in spallation thresholds by considering air cushioning among several possible causes, but they were unable to say that it was only air cushioning causing a 3:1 difference in some cases (Ref 10:3). The presence of the air not only decreases the projectile velocity but also alters the input

wave shape by an exponential buildup to the desired square pulse (Ref 10:4). They arrived at two conclusions. First, the experiments were conducted under such dissimilar conditions that any attempted correlation of a spallation threshold is meaningless. Secondly, the exploding foil method permits higher impact pressures, but the control of the experimental parameters can be more difficult than with an air gun (Ref 10:6).

V. Results and Discussion

This experimental investigation allowed for the study of 6061-T6 aluminum, and it revealed such things as single spalling, incipient spall pattern, spall threshold, spall propagation, and no hardening. These will be discussed in order.

Single Spalling

When spall occurred either internally or externally, it occurred only in a single zone parallel to the target front and back surfaces. A single spall for this experiment would indicate that only enough energy was available for one spall zone to form.

Waves of relatively weak intensity produce a single fracture zone (Ref 23:90). Single spalling is merely a special case of multiple spalling for the situation in which the maximum intensity of the transient stress lies between the critical, normal fracture stress and twice that value (Ref 23:91). The number of spalls increases with the linear dimensions of the experimental set-up (Ref 3:6).

Incipient Spall Pattern

Incipient spall, which was defined as internal spall, did not occur over a well-defined plane but was spread over a region which depended on the flyer velocity for each flyer thickness. The flyer thickness controlled the location of the spall zone. It was also determined that the average

incipient spall depth corresponded to about 1/5th of the sample thickness.

At the spall threshold (point where incipient spall begins), the flyer velocity will cause a thin incipient spall. As the flyer velocity was increased so was the width of the incipient spall until complete separation (spall) occurred. This was also observed by Blincow and Keller who found that the incipient spall zone was wider when the stress was high enough to cause damage even in regions where edge effects were interfering (Ref 2:261). But it should be kept in mind that it is not possible to completely eliminate all boundary effects.

The incipient spall locations were correlated with each flyer thickness. It was found that as the flyer thickness was decreased the incipient spall region was created nearer to the target free surface. A thickness increase would dictate a region farther from the free surface. This was as expected and can be seen graphically on the t - x plane where decreasing flyer thicknesses force the rarefaction waves in the target to shift towards the free surface. Keller and Trulio observed that cracks appeared in a region near the free surface of the target at a depth approximately equal to the driver plate thickness (Ref 15:3). So this would also indicate that as the driver plate thickness is decreased, the incipient spall region moves nearer to the free surface.

The average incipient spall depth was 1/5th the sample

thickness. This agrees with Keller and Blincow who found that the spall region in 6061-T6 aluminum extended from 1/6th to nearly 1/3rd of the thickness of the target (Ref 2:261).

Spall Threshold

Spall samples were those that visibly indicated spall after impact. If spall was not observed, the recovered targets were examined in the metallurgical laboratory. There they were classified as either incipient spall or no spall. The flyer velocity was plotted as a function of flyer thickness with damage classification as a parameter. The spall threshold for each flyer thickness was defined to be at the point of separation between damage and no damage. Damage was considered to be both spall and incipient spall while no damage was no spall. A curve was obtained by connecting the spall thresholds reached at each individual flyer thickness and the spall threshold for 6061-T6 Al was obtained. This spall threshold curve is plotted in Fig. 16, and the data used to obtain this curve can be found in Appendix E. This curve represents one of the major outcomes of this work; however, it must be remembered that these data were obtained in the presence of air. An equation that can be used to predict the spall threshold for 6061-T6 aluminum was obtained by a least squares fit

$$\dot{V} = C_1 \exp(-C_2 M) \qquad (16)$$

where $C_1 = 3.326$

$C_2 = 0.08505$

V = flyer velocity in mm/usec at the spall threshold

H = flyer thickness in mils

It would be better to plot pressure versus pulse duration, but the Mylar Hugonoit equation-of-state is not completely known; therefore, the spallation threshold data have been reported as flyer velocity versus flyer thickness. The Hugonoit of Mylar in the stress range of 3 to 30 kilobars has been determined and is considered to be the first accurate data that have been obtained for this material (Ref 20:1). For this study, the Mylar Hugonoit must be known in the neighborhood of 60 kilobars for a thorough analysis. Once this requirement has been fulfilled, then, the flyer velocity can be converted readily to the initial impact stress. This is accomplished graphically using the Mylar and 6061-T6 aluminum Hugonoits using the variables stress and particle velocity. The initial impact stress is often used as an experimental reference rather than the induced tension because the negative equation-of-state of the material in tension necessary for the calculation of tension are not available (Ref 17:361). Therefore, the length of time over which the maximum tension persists and its magnitude cannot be calculated accurately until a complete Hugonoit for Mylar is obtained.

While the Mylar data are only known to 30 kilobars, the Hugonoit of 6061-T6 aluminum is available at the

AF Weapons Laboratory to 60 kilobars and above. These data cover this alloy in both the elastic and plastic regions.

The experimental factor which contributes the most uncertainty is that of determining whether or not the target spalled (internally or externally) (Ref 15:175). Keller and Young found that this difficulty accounted for the scatter in threshold velocity as a function of flyer thickness and amounted to about ten per cent (Ref 16:15). The best remedy for this problem is to insure consistency of the damage criterion formulated. When other investigations are judged, the important idea to remember is that different investigators have used similar terminology but different criteria. The difficulty in determining damage or no damage for the recovered samples can be somewhat overcome by proper metallurgical techniques.

An effort was made to compare the spall threshold data obtained for 6061-T6 aluminum. This intention was troublesome because of various factors. This alloy had been dynamically impacted using various experimental techniques. Some investigators had used a gas gun while others had used exploding foils. In some cases data were obtained in a vacuum while in others air studies were performed. Different flyers and flyer thickness ranges had been considered. Various plate thickness ratios had been considered for pulse shape conservation. Even different designations of the same alloy had been impul-

sively loaded. Therefore, a direct data comparison was not feasible since other impact data for the alloy were obtained under different conditions.

Keller and Blincow conducted an impact threshold study with both flyer and target being 6061-T6 aluminum (Ref 2:261). They used both exploding foils and an air gun with flyers ranging from 10 mil up to 250 mil while this experiment was concerned with flyers ranging from 3 mil up to 10 mil. The spall threshold at 10 mil was a good point to correlate the data from the two experiments. After correcting for the difference in flyer materials and plate thickness ratio, the only remaining difference appeared to be that they performed their investigation in a vacuum. At 10 mil the spallation threshold obtained in this study was greater by a factor of two over the spallation threshold obtained by Keller and Blincow. Penning, Young, and Prindle obtained air gun data with 9.25 mil flyers impacting 6061-T4 aluminum targets (Ref 21:85). Their data were in agreement with Keller and Blincow.

Spall Propagation

The mechanism of spall formation and propagation in 6061-T6 aluminum was significant. The inclusions were observed to crack first followed by propagation from inclusion to inclusion until complete spallation resulted.

The microstructure of a material can profoundly influence the pattern of spalling (Ref 23:91). This experimental investigation was concerned with a structural

alloy, 6061-T6 aluminum, which was representative of impure metals and alloys. The inclusions present in the alloy were introduced in aluminum to give it strength, but dynamic loading of the alloy attacked these inclusions in such a way that the inclusions proved to be the point of vulnerability. These inclusions strongly influenced the pattern of spalling.

Inspection of various incipient spall specimens revealed that in some cases only cracking of the inclusions had occurred and none of the aluminum matrix. Other specimens indicated that cracks spread outward from the cracked inclusions. Therefore, it was deduced that the inclusions cracked first then the cracks propagated from inclusion to inclusion through the matrix material. These cracks propagated until a complete separation or spall resulted. Fig. 19 shows photomicrographs of cracked inclusions, and Fig. 20 shows the crack propagation from inclusions. The electron microprobe has been used to show that the inclusions in 6061-T6 Al contain large amounts of iron or silicon with lesser amounts of copper, manganese, chromium and magnesium present (Ref 5:4). Such a mixture is brittle relative to the aluminum matrix; therefore, dynamic impact would first result in the failure of the brittle inclusions. This situation is additionally complicated when the fact is introduced that a complicated stress state will be produced in both the inclusion and matrix when a shock wave interacts with these dissimilar

materials.

The effect of microstructure on crack initiation and propagation in 6061-T6 aluminum has also been performed by Dr. Barry Butcher of Sandia Corporation (Ref 5:1). He presented photomicrographs that he believed introduced the possibility that crack propagation is somewhat influenced by the inclusions; there seemed to be a greater number of inclusions in regions where cracks had formed (Ref 5:4). He concluded that spall in 6061-T6 aluminum may well be influenced, if not completely controlled by impurities (Ref 5:5). Another related article by personnel at Sandia Corporation states that spall is thought to be nucleated at inclusions and at precipitates as interfacial contact between the matrix and the particle is destroyed by shock wave action (Ref 6:988).

For impure metals and alloys, Moss and Glass found that cracks were observed to start at inclusions; the cracks then propagated through the material with simultaneous plastic deformation (Ref 19:7). In a paper presented at a conference, Moss, Glass, and Golaski stated that microscopic studies indicated that spalls began at inclusions, and the propagation of the spall surface is a function of the number and types of inclusions (Ref 8:115).

An attempt was made to determine if the cracking in the alloy was transgranular or intergranular. This venture to see if the cracks followed or crossed the grain boundaries proved to be unsuccessful. This was attributed to

the fact that the inclusions and the cracks were attacked by the various etchants used before the grain boundaries could be located.

Hardness

Recovered targets were examined for changes in hardness and microstructure. No significant change in hardness was observed, and no phase transitions were observed. Some of the literature specifys that the hardness of metals and alloys increases with increasing shock pressure (Ref 1:197, Ref 7:35). An average temperature rise of 350° was calculated for the recovered specimens. It can be concluded that this temperature rise applied for the short periods of this experimental arrangement would not affect the hardness.

VI. Conclusions

A criterion to predict material spallation was established for the structural alloy, 6061-T6 aluminum. The spall threshold in this material was experimentally measured and can be calculated. The empirical equation that can be used as a criterion to allow spall predictions for 6061-T6 is

$$V = C_1 \exp(-C_2 M) \qquad (16)$$

where

$C_1 = 3.326$

$C_2 = 0.08505$

V = flyer velocity in mm/usec at the spall threshold

M = flyer thickness in mils

Besides formulating a spall criterion, an additional result of significance was reached. The mechanism of incipient spall formation in 6061-T6 aluminum was microscopically observed. This mechanism can be extended to apply to the initiation of incipient spall in impure metals and alloys. Photomicrographs revealed cracks that seemed to start at inclusions, brittle compared to matrix material, during the early stages of incipient spall and that seemed to propagate from inclusion to inclusion during later stages of incipient spall formation.

This investigation used experimental techniques that can be extended to study the response of other materials to shock waves. Once materials with different properties have been researched, it may then be possible to predict material spallation by a general spall model.

VII. Recommendations

Vacuum Study

A spallation threshold investigation should be performed with impact occurring in a vacuum. There should be two main objectives in this recommended study; these objectives are the following: (1) perform an identical analysis to this thesis study, and (2) determine the critical flyer thickness where air cushioning ceases to be a major problem. The first objective should provide a vacuum spallation threshold that would be relative to the air spallation threshold; the second objective would lead to a criterion that would specify when a dynamic response determination should be performed in a vacuum or in air. Included in the second objective should be an attempt to determine the critical flyer-target separation distance.

Multiphase Metals

After the above investigation has been completed, research should be directed towards spallation in multiphase metals. This study has been proposed by Lt. A. I. Blechman of the Air Force Weapons Laboratory. Reliable sources indicate that in a two-phase material, incipient spall tends to begin in the more brittle phase. This is because the mechanical properties are different. The stress wave that propagates through the material causes a different amount

of strain into different phases. Normally, this is relieved by plastic deformation; however, in the time interval associated with the passage of such a wave, plastic deformation does not occur. This, together with the complicated state of stresses that normally exist at an interface between two phases, causes failure to begin in the more brittle phase. It is proposed that a two-phase material such as brass be impacted with mylar flyers using the plate slap equipment at the Pulse Power Facility to generate incipient spall.

Bibliography

1. Appleton, A. S. "The Metallurgical Effects of Shock Waves." Applied Materials Research, 4:195-201 (October 1965).

2. Blincow, D. W. and D. V. Keller. "Experiments on the Mechanism of Spall." Symposium on Dynamic Behavior of Materials, 5:252-263 (September 1962).

3. Broberg, K. B. The Broberg Lectures. Report No. 59-1. Golden, Colorado: Colorado School of Mines Research Foundation, Inc, July 1959.

4. Butcher, B. M. Private Communication.

5. Butcher, B. M. Spallation in 6061-T6 Aluminum. SC-DC-66-2448. Albuquerque: Sandia Laboratory.

6. Butcher, B. M., et al. "Influence of Stress History on Time Dependent Spall in Metals." AIAA Journal, 2:977-990 (June 1964).

7. Duvall, G. E. Some Properties and Applications of Shock Waves. Poulter Laboratories Technical Report 006-60. Menlo Park, California: Stanford Research Institute, October 1960. AD 250 564.

8. Glass, C. M. "Effects of Explosive Loading on Single Crystals and Polycrystalline Aggregates." Response of Metals to High Velocity Deformation, 9:115-137 (July 1960).

9. Guenther, A. H. "Production of Strong Shocks in Plastics by Ultra-Short Impulsive Loading." Symposium on Dynamic Behavior of Materials, 5:219-250 (September 1962).

10. Hartman, W. F. An Explanation of the Inconsistency of Spallation Thresholds as Determined by Various Observers. SCDR 65-61. Albuquerque: Sandia Corporation, February 1961.

11. Herrmann, W., et al. Stress Wave Propagation and Spallation in Uniaxial Strain. Technical Documentary Report No. ASD-TDR-62-399. Wright-Patterson Air Force Base, 0410: Aeronautical Systems Division, September 1962. AD 288 885.

12. Holtzman, A. H. and G. R. Cowan. "Strengthening of Austenitic Manganese Steel." Response of Metals to High Velocity Deformation, 9:481-482 (July 1960).

13. Karnes, C. Private Communication.

14. Keller, D. V. and J. R. Penning, Jr. Exploding Foils — The Production of Plane Shock Waves and the Acceleration of Thin Plates. D2-90094. Seattle: The Boeing Company, December 1961.

15. Keller, D. V. and J. G. Trulio. "Mechanism of Spall in Lucite." Journal of Applied Physics, 34:172-175 (January 1963).

16. Keller, D. V. and D. M. Young. A Method for Determining Spallation Criteria in Solids. Technical Documentary Report No. AFSWC-TDR-61-102. Kirtland Air Force Base, New Mexico: Air Force Special Weapons Center, November 1961. AD 270 652.

17. Lundergan, C. D. "Spall Fracture." Proceedings of Symposium on Structural Dynamics Under High Impulse Loading, ASD-TDR-63-140:357-380 (May 1963). AD 408 777.

18. McQueen, R. G. "Laboratory Techniques for Very High Pressures and the Behavior of Metals Under Dynamic Loading." Metallurgy at High Pressures and High Temperatures, 22: 44-129 (February 1963).

19. Moss, G. and C. M. Glass. Some Microscopic Observations of Cracks Developed in Metals by Very Intense Stress Waves. Ballistic Research Laboratories Technical Note No. 1312. Aberdeen Proving Ground, Maryland: Ballistic Research Laboratories, April 1960. AD 237 943.

20. Penning, J. R. and F. W. Davies. Hugonoit Equation of State of Mylar. Boeing Document D2-125304-1. Seattle: The Boeing Company.

21. Penning, J. R., et al. Negative Equation of State and Spall Criteria. Technical Documentary Report No. RTD-TDR-63-3039. Kirtland Air Force Base, New Mexico: Air Force Weapons Laboratory, September 1963.

22. Percy, J. H. "Wave Propagation in Uniaxial Strain." Proceedings of Symposium on Structural Dynamics Under High Impulse Loading, ASD-TDR-63-140:123-134 (May 1963). AD 408 777.

23. Rinehart, J. S. "Fracturing by Spalling." Wear —Usure —Verschleiss, 7:315-329 (July-August 1964).

24. Rinehart, J. S. Practical Countermeasures for the Prevention of Spallation. AFSWC-TR-60-7. Kirtland Air Force Base, New Mexico: Air Force Special Weapons Center, February 1960. AD 236 719.

25. Rinehart, J. S. and J. Pearson. Behavior of Metals Under Impulsive Loads. Cleveland: The American Society for Metals, 1954.

26. Rinehart, J. S. and J. Pearson. Some Tensile Fractures Generated by Impulsive Compressional Loading. NOTS-TM-346. China Lake, California: U. S. Naval Ordnance Test Station, January 1952. AD 493 328.

27. Walsh, J. M., et al. "Shock Wave Compressions of 27 Metals. Equations of State of Metals." The Physical Review, 108:196-216 (October 1957).

28. Weis, C., et al. Analysis of Flying Plate Experiments. Technical Documentary Report No. AFSWC-TDR-61-74. Kirtland Air Force Base, New Mexico: Air Force Special Weapons Center, January 1962.

29. Wunsch, D. C. and A. H. Guenther. Field Shift in High — Speed Rotating Mirror Framing Cameras. Technical Documentary Report No. AFSWC-TDR-61-76. Kirtland Air Force Base, New Mexico: Air Force Special Weapons Center, September 1962.

30. Wunsch, D. C., et al. Acceleration of Thin Plates by Exploding Foil Techniques. Technical Documentary Report No. AFSWC-TDR-61-75. Kirtland Air Force Base, New Mexico: Air Force Special Weapons Center, January 1962.

Appendix A

Literature Survey

The references listed in the bibliography are the ones most applicable to this investigation, and they are representative of publications in the field of shock waves in solids, especially fracture and spall. Since other literature is available, this bibliography is by no means complete. The literature search performed was able to get the references to converge using two different sources. First, various literature surveys were used such as Survey of Spallation Literature by Z. Reider and Impact Physics by Sandia Corporation. Both of these contained information up until 1959. Bibliographies were obtained from the Defense Documentation Center and Battelle Memorial Institute containing information for the last twenty years. The DDC Bibliography contained only Government literature, and the Battelle survey had both Government and periodical literature. The Engineering Index was researched for the period of 1959-1967. Secondly, bibliographies contained in acquired articles were followed through. Thus, by using the literature surveys and bibliographies from articles, the point was reached where the same articles were being referenced.

Appendix B

Aluminum Alloy Designation

The designation 6061 aluminum refers to a wrought aluminum alloy having a nominal composition of 0.6 per cent Si, 0.25 per cent Ca, 1.0 per cent Mn, 0.25 per cent Cr, and 97.9 per cent Al. The suffixed designation TX,X being any number, refers to the heat treatment given the alloy. All 6061-TX alloys have been solution-heat-treated at 970 degrees Fahrenheit for two to three hours. If aged at 350 degrees Fahrenheit for six to eight hours, the designation is T6 (Ref 21:149).

Appendix C

Exploding Foil Assembly

The nomenclature for the exploding foil assembly used for this experiment was A 0.25 Al (3/2 x 3/2) MYLAR. The elements of the exploding foil assembly are a back-up block, copper electrodes, an aluminum foil, a Mylar sheet, and a barrel, which is made up of two sections. The first figure in this appendix shows the relative position in the assembly for each element. The following figures in this appendix give specifications for each element in the assembly. A detailed discussion is available in the experimental procedure section.

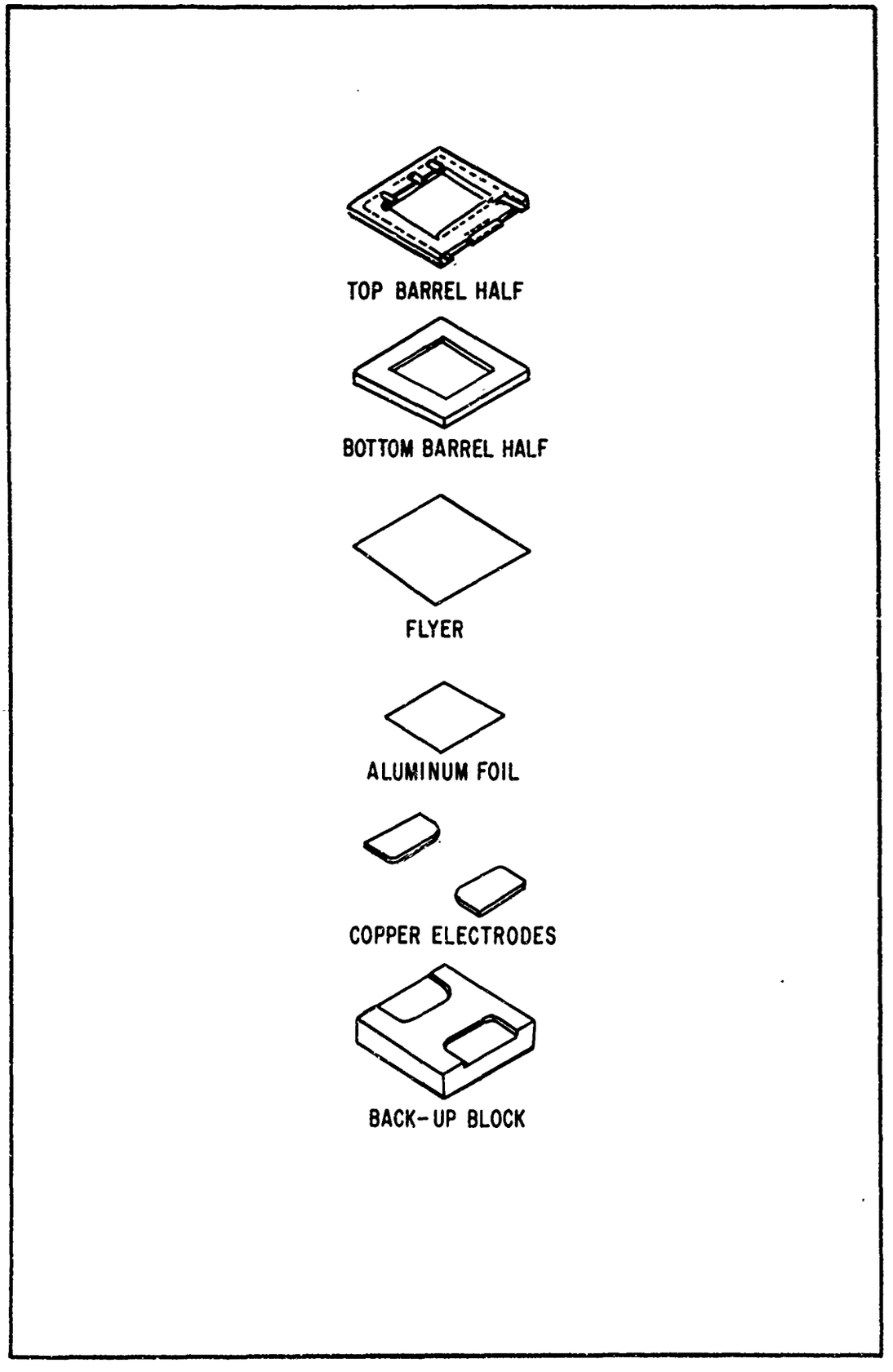

Fig. 21. Elements of A Exploding Foil Assembly

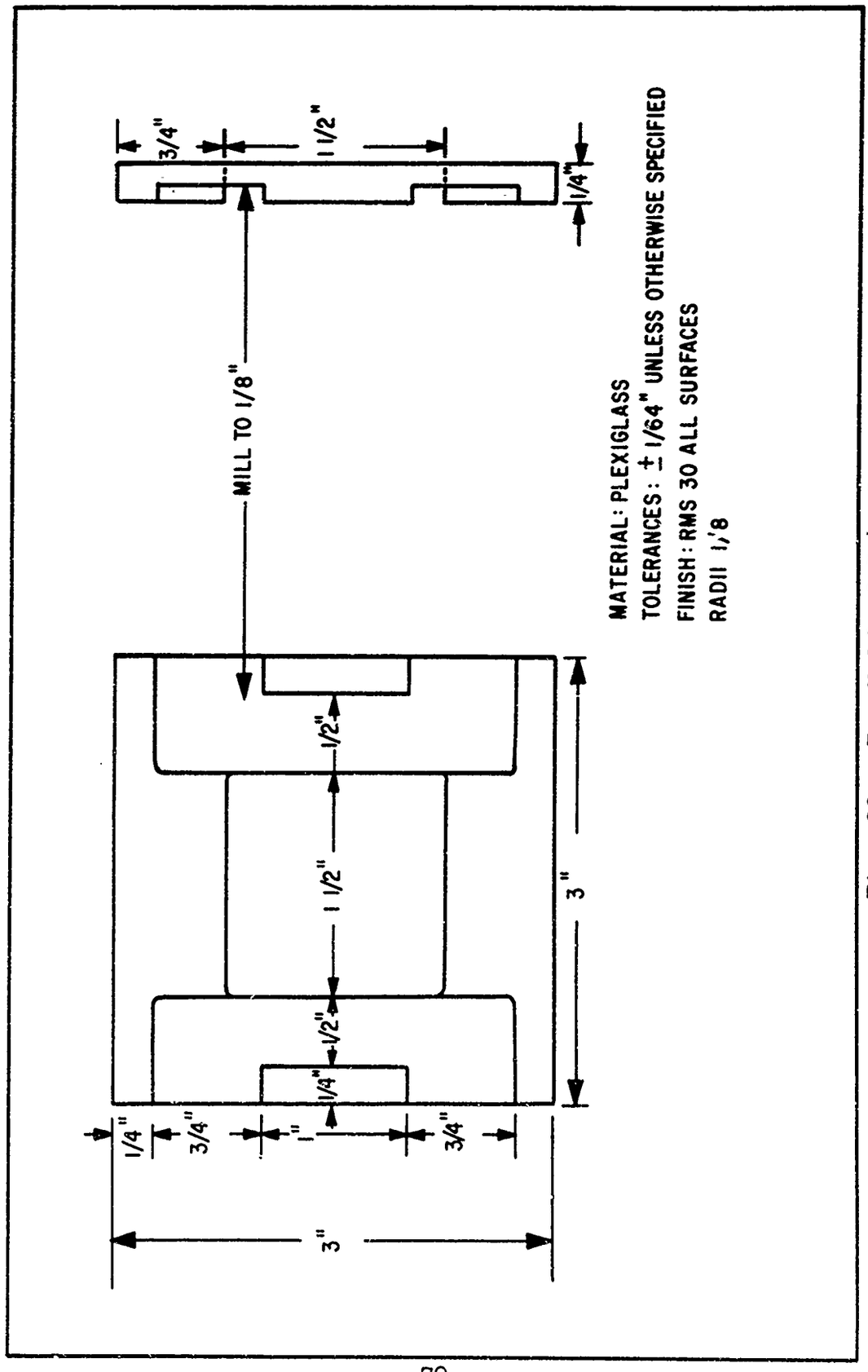

Fig. 22. Top Half of Barrel

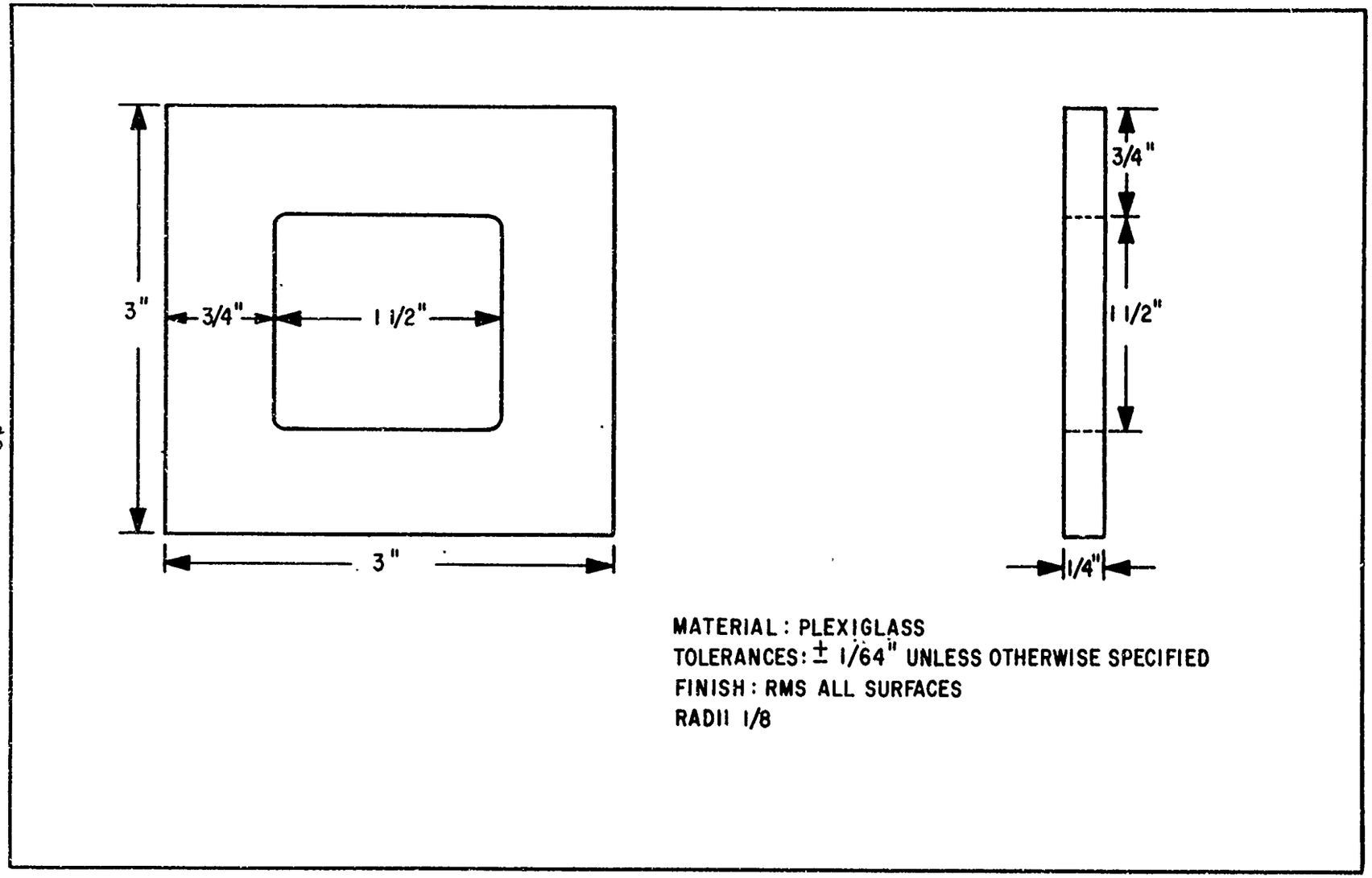

Fig. 23. Bottom Half of Barrel

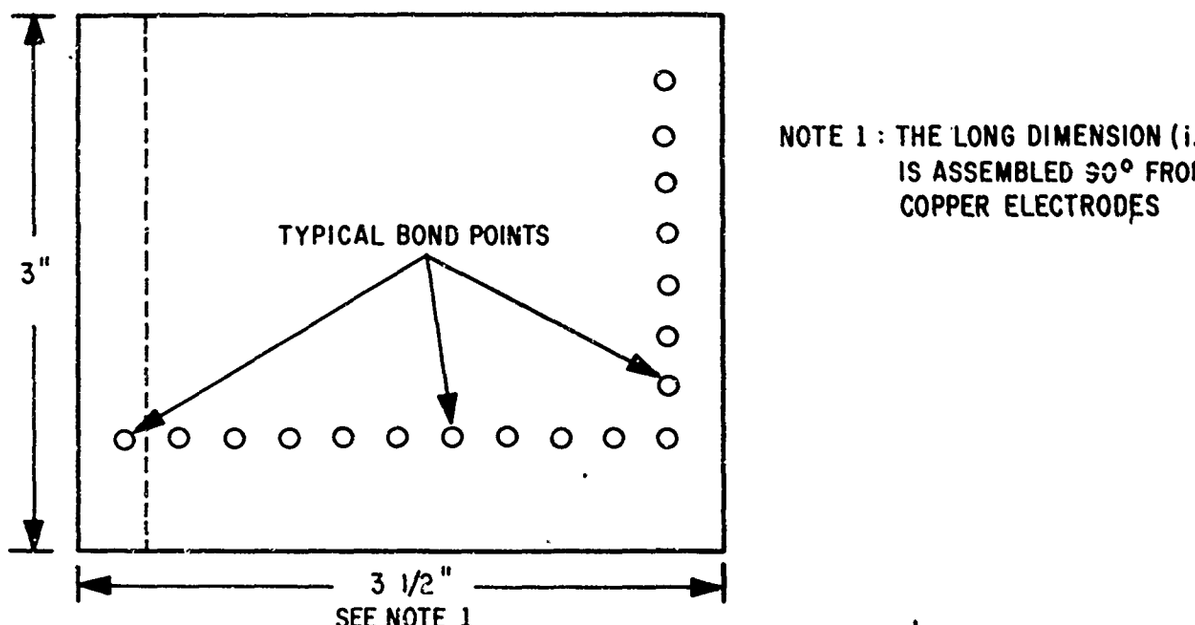

Fig. 24. Mylar Flyer

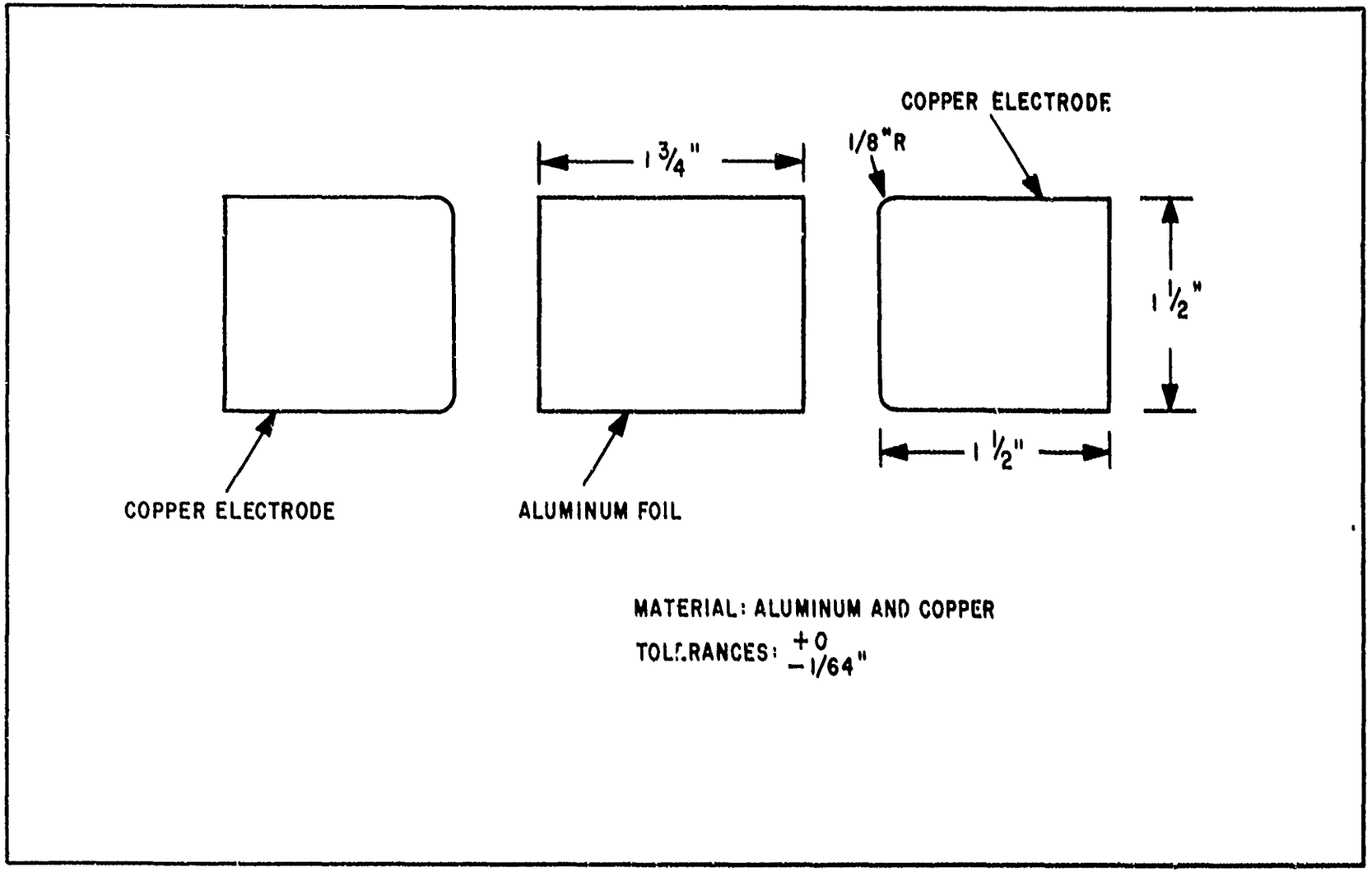

Fig. 25. Aluminum Foil and Copper Electrodes

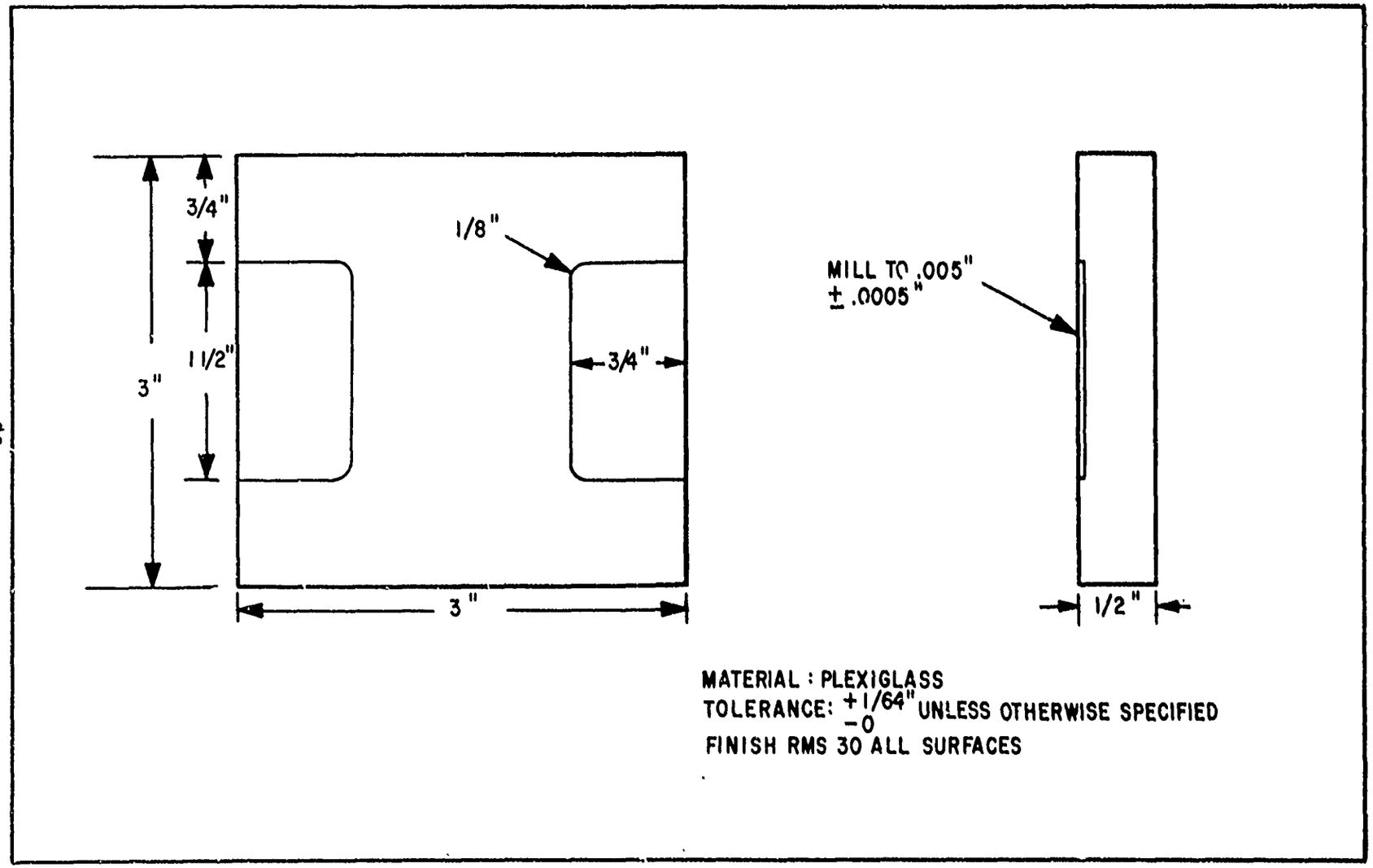

Fig. 26. Back-Up Block

Appendix D

Metallurgical Procedures

Control Sample

A control sample of 6061-T6 aluminum was found to exhibit a hardness range of 52.5 to 58 Rockwell B, with an average of 55.25 Rockwell B. The average grain size was determined to be ASTM 6 1/2. This indicates that the average grain diameter is approximately 0.00149 inch and that there are approximately 48 grains per square inch at 100X. There did not appear to be any unusual deformation characteristics within the control sample.

Sectioning

Recovered 6061-T6 targets were sectioned as depicted in Fig. 15. The metallurgical specimens were extracted from the center region of the impacted target; samples were approximately 0.75 inch by 0.25 inch. Potential damage induced by sectioning was kept to a minimum by using a jewelers saw. The sectioned samples were mounted in a Bakelite molding compound; they were mounted to permit observation perpendicular to the motion of the shock wave through the target.

Polishing

A flat surface was provided by rough grinding. Gross effects of sectioning were removed using silicon carbide

discs of 120 grit followed by 180 grit. Fine grinding was performed on successively finer silicon carbide discs of 240, 320, 400, and 600 grit. Final polishing was conducted with a 15 micron diamond compound and subsequently with a one micron diamond compound. Finish polishing was conducted by vibratory polishing techniques using a 0.3 micron alumina slurry. Care had to be taken in polishing to insure that the harder inclusions were not removed from the softer base material.

Etching

Micro-constituent etching was accomplished using the following etchant: 5 ml hydrofluoric acid, 10 ml sulfuric acid, and 170 ml water. A chemical etchant to determine the grain boundaries but not react with the constituents has not been found.

Microscopic Observations

Most stages of incipient spall were viewed microscopically at about 50X to 100X. The early stages of incipient spall usually required a magnification of about 1000X. In most cases only polishing and not etching was satisfactory in revealing incipient spall. The polishing operation causes a layer of deformed metal to be produced on the surface which distorts the true micro-structure of the material. By lightly etching the specimen, this layer can be removed without delinerating the grain boundaries or dissolving the inclusions.

Hardness Testing

Planarity-One, P-1, samples that exhibited either incipient spall or no spall were tested for hardness. A Knoop Diamond Indentor and a 0.1 kilogram weight were used with a Wilson Tukon Micro-hardness Tester. Observations were made at 200X, and hardness readings were taken across the specimens at intervals of approximately 0.005 millimeters.

Appendix E

Table of Experimental Data

Table I

Spall Threshold Data for Mylar Flyers Impacting on 32 mil 6061-T6 Aluminum Target for Planarity-One Shots Only

Shot Number	Flyer Thickness (mil)	Flyer Velocity (mm/usec)	Damage
0524	10	1.42	No Spall
0531	10	1.86	Spall
0539	5	2.42	Incipient Spall
0544	7.5	1.84	Incipient Spall
0558	5	2.12	No Spall
0559	5	2.06	No Spall
0560	7.5	1.39	No Spall
0561	10	1.56	Incipient Spall
0564	7.5	1.69	No Spall
0570	5	2.48	Spall
0571	5	2.41	Spall
0575	5	1.91	No Spall
0576	7.5	1.88	Spall
0578	7.5	1.85	Incipient Spall
0579	10	1.76	Spall
0580	10	1.75	Incipient Spall
0583	10	1.52	Incipient Spall
0586	5	2.17	Incipient Spall
0588	7.5	1.62	No Spall
0589	5	2.36	Incipient Spall
0597	5	2.17	Incipient Spall
0604	3	3.07	Spall
0611	3	2.64	No Spall
0616	10	1.48	No Spall
0617	10	1.46	No Spall
0618	10	1.33	No Spall
0619	10	1.59	Incipient Spall
0620	3	2.84	Incipient Spall
0621	3	2.88	Incipient Spall
0622	3	3.03	Spall
0623	3	2.89	Incipient Spall
0628	5	2.42	Incipient Spall
0642	7.5	1.56	No Spall
0646	7.5	1.68	Incipient Spall
0675	7.5	1.89	Incipient Spall
0676	7.5	2.02	Spall
0677	7.5	2.01	Spall

Unclassified
Security Classification

DOCUMENT CONTROL DATA - R & D

(Security classification of title, body of abstract and indexing annotation must be entered when the overall report is classified)

1. ORIGINATING ACTIVITY *(Corporate author)*
Air Force Institute of Technology (AFIT-SE)
Wright-Patterson AFB, Ohio 45433

2a. REPORT SECURITY CLASSIFICATION
Unclassified

2b. GROUP

3. REPORT TITLE
Determination of Spallation Thresholds by Exploding Foil Techniques

4. DESCRIPTIVE NOTES *(Type of report and inclusive dates)*
AFIT Thesis

5. AUTHOR(S) *(First name, middle initial, last name)*
Jose R. Baca
Captain USAF

6. REPORT DATE	7a. TOTAL NO. OF PAGES	7b. NO. OF REFS
June 1968	88	30

8a. CONTRACT OR GRANT NO.	9a. ORIGINATOR'S REPORT NUMBER(S)
b. PROJECT NO. N/A	GNE/PH/68-2
c.	9b. OTHER REPORT NO(S) *(Any other numbers that may be assigned this report)*
d.	

10. DISTRIBUTION STATEMENT
This document is subject to special export controls and each transmittal to foreign governments or foreign nationals may be made only with prior approval of the Dean of Engineering, Air Force Institute of Technology (AFIT-SE), Wright-Patterson AFB, Ohio 45433

11. SUPPLEMENTARY NOTES	12. SPONSORING MILITARY ACTIVITY

13. ABSTRACT Exploding foil techniques were used to accelerate a Mylar Flyer at a controlled velocity to produce a plane, longitudinal shock wave in 6061-T6 aluminum, and the interaction of the wave with the target free surface was studied.

Flyer velocity and planarity were determined by high-speed, photographic techniques. The spall threshold was determined as a function of flyer velocity and thickness. A criterion was formulated to predict the spall threshold.

Microscopic analyses revealed the mechanism of incipient spall in 6061-T6 aluminum to be cracks which propagated from inclusions in the matrix material.

DD FORM 1 NOV 65 1473

Unclassified
Security Classification

Unclassified
Security Classification

14. KEY WORDS	LINK A		LINK B		LINK C	
	ROLE	WT	ROLE	WT	ROLE	WT
Exploding Foil						
Shock Wave						
6061-T6 Aluminum						
Spall Threshold						

Unclassified
Security Classification